MAGYAR ÁLLAMI
EÖTVÖS LORÁND
GEOFIZIKAI INTÉZET

EÖTVÖS LORÁND
GEOPHYSICAL INSTITUTE
OF HUNGARY

GEOFIZIKAI KÖZLEMÉNYEK

GEOPHYSICAL TRANSACTIONS

ВЕНГЕРСКИЙ
ГЕОФИЗИЧЕСКИЙ
ИНСТИТУТ
ИМ Л. ЭТВЕША

ГЕОФИЗИЧЕСКИЙ
БЮЛЛЕТЕНЬ

CONTENTS

VOL. 33. NO. 1. JULY 1987. (ISSN 0016-7177)

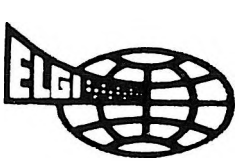

BUDAPEST

TARTALOMJEGYZÉK

СОДЕРЖАНИЕ

GEOPHYSICAL TRANSACTIONS 1987
Vol. 33. No. 1. pp. 3–9

POSSIBILITIES TO REALIZE HIGHER EFFICIENCY IN GEOPHYSICAL INTERPRETATION

Ferenc STEINER*

If the algorithm of interpretation of geophysical data systems contains, in an explicit or implicit manner, statistical tools, it is deemed advisable to apply such statistical procedures (estimations, fitting techniques, etc.) which have great efficiency for a large range of probability distribution types. The present paper deals, with this special point of view and, in a concise manner, with the statistical procedures based on the generalized most frequent value.

Keywords: probability, statistical distribution, robust estimation, Danish method, least-squares analysis

1. Introduction

Algorithms of geophysical interpretation often contain (in an explicit or implicit manner) statistical components, too. This short paper deals with cases when this constituent part is some sort of fitting.

If there are K equations among the components of the parameter vector $\bar{p} = p_1, p_2, \ldots, p_j, \ldots, p_J$ to be determined, we have to fulfil exactly

$$A_k(\bar{p}) = 0 \qquad (k = 1, \ldots, K)$$

with given analytical expressions $A_k(\ldots)$. (We write $K=0$ if there are no equations to be fulfilled.)

If $\bar{y}_i$ denotes the exactly known vector-variable, its components are, in the case of a fitting with m variables,

$$y_{i1}, y_{i2}, \ldots, y_{im}.$$

The z_i results of the measurements consist of the "exact value" $T(\bar{p}; \bar{y}_i)$ ($T(\ldots)$ is an a priori known analytical expression) and the "error" x_i ($i = 1, \ldots, n$ if n is the number of measured data). It depends on the type of probability distribution of errors x_i what sort of fitting will give optimal interpretation from the statistical point of view.

* Department of Geophysics, Technical University for Heavy Industry, Miskolc, Egyetemváros, H-3515, Hungary
Manuscript received: 26 November, 1986

2. Fitting by most frequent value

For the sake of simplicity let us suppose a symmetrical distribution of errors $f(x)$ with a parameter of scale $S=1$. The symmetry point lies, of course, at zero, $f(x)$ being the probability density function of errors.

Let us suppose that careful investigation of a great number of large samples justifies that the density function has the analytical form:

$$f_G(x) = \frac{1}{\sqrt{2\pi}} e^{-\frac{x^2}{2}} \tag{1}$$

i.e. the errors x_i have a Gaussian distribution. We have in this case to fulfil the demand

$$\sum_{k=1}^{K} \lambda_k A_k(\bar{p}) + \sum_{i=1}^{n} x_i^2 = \text{minimum} \tag{2}$$

to get the vector of parameters $\bar{p}$ as exact as possible, supposing that the appearance of outliers can be absolutely excluded. (λ_k denotes for $k=1, \ldots, K$ the well known Lagrange multipliers.) However, if the investigation of the type of probability distribution of errors x_i results in a density function

$$f_a(x) = N \cdot (1+x^2)^{-\frac{a}{2}} \tag{3}$$

for some a value ($1<a<\infty$) as an adequate model for the actual distribution (the explicit formula for the norming factor N is given in [Csernyák and Steiner 1982]), then the solution of the condition

$$\exp\left[\sum_{k=1}^{K} \lambda_k A_k(\bar{p})\right] \cdot \prod_{i=1}^{n} (1+x_i^2) = \text{minimum} \tag{4}$$

gives the optimal $\bar{p}$ (i.e. with minimal asymptotic variance; for $K=0$ [see Steiner 1985]).

The above mentioned statements are condensed in *Fig. 1.*

In most cases of fitting the following form of $T(\bar{p}; \bar{y})$ is accepted:

$$T(\bar{p}; y) = \sum_{j=1}^{J} p_j \cdot T_j(\bar{y}). \tag{5}$$

For simplicity $K=0$ but from now on S is allowed to be arbitrary. After logarithmization of Eq. 4 and derivation according to p_j we shall have formally the same equation system as by fulfilling the least squares condition with a priori weights; the weights, however, must now be calculated according to

$$\varphi(x_i) = \frac{(k\varepsilon)^2}{(k\varepsilon)^2 + x_i^2} \tag{6}$$

where ε denotes the dihesion of the data system x_i [see e.g. Steiner 1985], the

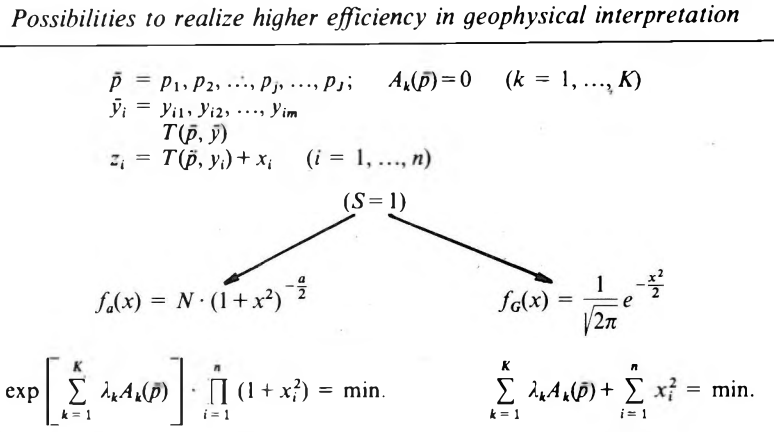

Fig. 1. Schema of optimal fitting techniques for different types of probability distributions of the error x

1. ábra. Optimális kiegyenlítési eljárások különböző típusú valószínűségi hibaeloszlásra

Рис. 1. Оптимальные способы выравнивания при различных типах вероятностного распределения ошибок.

value of k corresponds to the actual value of a, with $f_a(x)$ being the density function of the best, i.e. of the most adequate, model. (The function $k(a)$ can be determined, of course, once for all, see [STEINER 1985]. Some values are: $k(2) = 1$; $k(4.4) = 1.9$; $k(6.2) = 2.4$ and $k(8) = 2.8$.) The value x_i, however, as the difference between the measured and the calculated value, depends also upon $\bar{p}$ and, consequently, the solution of the equation system is to be carried out as an iteration—but every step of the iteration can be calculated by means of the standard program for weighted least squares fitting. An additional program gives in a few iteration steps the approximation of the dihesion ε—and we have defined completely the algorithm we call "fitting according to the generalized most frequent value".

3. Examples

This new type of fitting is to be compared, on the one hand, with the conventional least squares fitting, and on the other hand with other robust and resistant methods. For clarity and in order to consider at the same time a high variety of distribution types we make the comparisons on the ground of the $f_a(x)$ distribution family defined in Eq. 3 (for $a > 1.7$). It is well known that $a = 2$ corresponds to the Cauchy distribution, $a = \infty$ to the Gaussian distribution. If the actual distributions are expected between these two types (and nothing more is known about the types), then the most appropriate choice is $k = 1.9$. If more information is known about the most probable a-range, the middle a-value of this shorter interval will guarantee for us an efficiency of 100 per cent or a value very near to this optimum.

The oldest robust procedure minimizes the sum of the absolute differences; in the case of $T=$const. this corresponds to the calculation of the sample median. I have chosen from the more modern robust procedures, for the sake comparison, the so-called "Danish method" [KRARUP and KUBIK 1983] because Hungarian surveyors seem to show very much interest in this procedure [DETREKŐI 1986]. Although there are some different variants of this method, the most often used weight function by the Danish method is:

$$\varphi(x_i) = \begin{cases} 1, & \text{if} \quad x_i < b \\ \exp\,(1-(x_i/b)^2), & \text{if} \quad x_i \geq b, \end{cases} \tag{7}$$

where

$$b = \frac{c \cdot \text{med}\,|x_i|}{0.6745}.$$

The most direct way to test the economy of the method is to calculate the efficiency e. Namely, the reciprocal of this value gives a very important ratio: how many times more data are necessary to result in the same reliability using an arbitrary statistical procedure, compared with the optimal one. The efficiency is to be calculated as the quotient of the two asymptotic variances belonging to both procedures in question:

$$e = \frac{A^2_{\text{opt}}}{A^2}. \tag{8}$$

If $S=1$ holds

$$A^2 = \frac{\int\limits_{-\infty}^{\infty} \psi^2(x) f(x)\,\mathrm{d}x}{\left[\int\limits_{-\infty}^{\infty} \psi'(x) f(x)\,\mathrm{d}x\right]^2} \tag{9}$$

(see e.g. [STEINER 1985]) with $\psi(x) = x \cdot \varphi(x)$, and one can easily verify [HAJAGOS 1985] for the distribution family $f_a(x)$ defined by Eq. 3 that

$$A^2_{\text{opt}} = \frac{a+2}{a \cdot (a-1)}. \tag{10}$$

For the sample median we can get the asymptotic scatter simply as the reciprocal of $2f_a(0)$.

Figure 2 shows the curves of efficiencies versus $1/(a-1)$, calculated as discussed above. The Danish method gives two curves for different c-values: according to the literature $c=3$ is the most frequently used value of this parameter; a practical example, however, is shown by KRARUP and KUBIK [1983] to be $c=1.5$, and therefore the efficiency curve was constructed using this c-value, too.

As the asymptotic variance of arithmetical means exists only for $a>3$ and

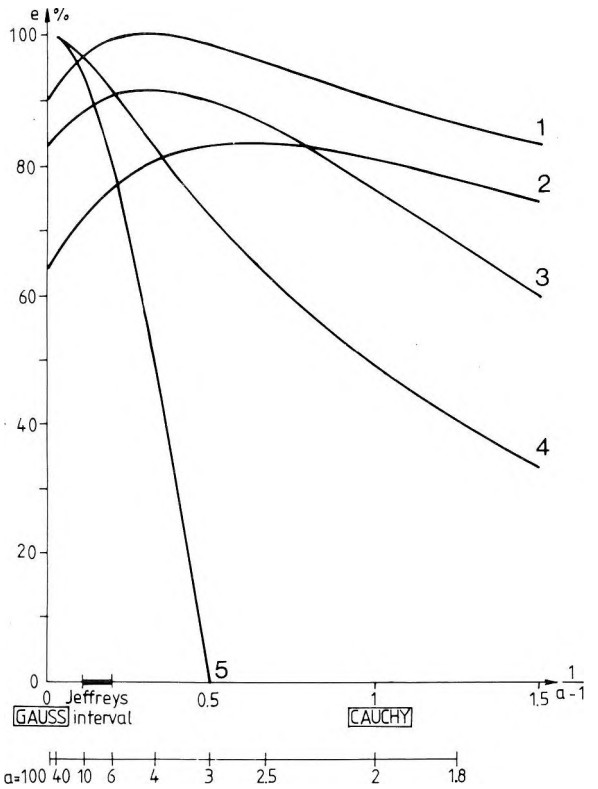

Fig. 2. Efficiences of some statistical procedures for a large range of probability distribution types
e — efficiency (%), 1/(a − 1) — type parameter of the probability distribution of errors; 1 — fitting according to the generalized most frequent value, k = 1.9; 2 — minimization of absolute differences; 3 — Danish method, c = 1.5; 4 — Danish method, c = 3; 5 — least squares fitting

2. ábra. Néhány statisztikai módszer hatékonysága a valószínűségi eloszlások széles skálájára
e — hatásfok (%), 1/(a − 1) — az eltérések (hibák) eloszlásának típusparamétere; 1 — általános leggyakoribb érték szerinti kiegyenlítés, k = 1,9; 2 — abszolút eltérések minimalizálása (medián); 3 — dán módszer, c = 1,5; 4 — dán módszer, c = 3; 5 — legkisebb négyzetek módszere

Рис. 2. Эффективность некоторых статистических методов в широком диапазоне вероятностных распределений
e — эффективность (%); 1/(a − 1) — типовой параметр распределения отклонений (ошибок); 1 — выравнивание по наиболее частому генеральному значению, k = 1,9; 2 — сведение абсолютных отклонений к минимуму (медиана); 3 — датский способ, c = 1,5; 4 — датский способ, c = 3; 5 — способ наименьших квадратов.

its value is in this case $1/(a-3)$ [CSERNYÁK–STEINER 1982], the efficiency curve starts at 100% (versus $1/(a-1)$)but rapidly decreases to zero. Compared with this behaviour, an enormous gain is offered by the Danish method applying $c=3$. If $c=1.5$ is used instead of $c=3$ the effectiveness increases considerably in the neighbourhood of the Cauchy distribution (from about 50%, to about 80%), the effectiveness in the case of Gaussian distribution, however, decreases to 83% (but this value is still considerably greater than the efficiency value of about 64% of the sample median). The efficiency of the generalized most frequent value is greater than 90% in the whole range from the Gauss type to the Cauchy type (i.e. for $a>2$), and therefore the economic advantages are obvious. If previous investigations concerning the type of actual probability distributions result in a value of $1/(a-1)$ whether near to zero or near to unity, we have only to choose the suitable value of k, i.e. according to the function $k(a)$, to reach an effectiveness very near to 100 per cent (as mentioned yet above). Both cases may occur in practice, not only in geophysics but also, for example, in astronomy: the data system of SHORT [1963] refers to Cauchy distribution (determined with the know-how belonging to the University of Miskolc); on the other hand, the copybook example of the least squares monograph of Linnik (see Table 6 in [LINNIK 1961]) can really be regarded as nearly Gaussian (the adequate value of a is indeed great) if we can disregard a small loss—say, one or two per cent—in the efficiency.

Finally, the economically very important role of the efficiencies should be emphasized. For instance, if we use a procedure with an efficiency of only 50 per cent, it means nothing less than our having thrown out half of our expensively measured data.

Acknowledgements

The author is indebted to J. Somogyi (director of the Geodetical and Geophysical Research Institute Ac. Sci. Hung.), and to professors L. Csernyák (College of Finance and Accountancy, Budapest) and B. Hajagos (Higher Institute of Digital Control for Chemical Engineering, Kazincbarcika) for their valuable help and discussions.

REFERENCES

CSERNYÁK L., STEINER F. 1982: Untersuchungen über das Erfüllungstempo des Gesetzes der großen Zahlen. Publ. of the Techn. Univ. for Heavy Ind., Miskolc Series A, Mining, **37,** 1–2

DETREKŐI Á. 1986: Consideration of robust errors in the processing of survey data (in Hungarian). Geodézia és Kartográfia **38,** 3, pp. 155–160

HAJAGOS B. 1985: Die verallgemeinerten Studentschen t-Verteilungen und die häufigsten Werte. Publ. of the Techn. Univ. for Heavy Ind., Miskolc Series A, Mining, **40,** 1–4, pp. 225–238

KRARUP T., KUBIK K. 1983: The Danish method; experience and philosophy. Seminar Math. models of geodetic (photogrammetric) point determination with regard to outliers and systematic errors (ed. by F. E. Ackermann). Deutsche Geodätische Kommission Reihe A, Nr. 98, München

LINNIK J. W. 1961: Die Methode der kleinsten Quadrate in moderner Darstellung. Deutscher Verlag der Wissenschaften, Berlin, 31 p.

SHORT J. 1763: Second paper concering the parallax of the sun etc. Philos. Trans. Roy. Soc., London **53,** pp. 300–343

STEINER F. 1985: Robust estimations (in Hungarian). Tankönyvkiadó, Budapest, 172 p.

HATÁSFOKNÖVELÉSI KÉRDÉSEK A GEOFIZIKAI ÉRTELMEZÉSBEN

STEINER Ferenc

A terepmérések által szolgáltatott egyre nagyobb geofizikai adatrendszerek kötelességünkké teszik, hogy minél hatásosabban nyerjük ki az azokban levő információkat. Ha értelmezési algoritmusunk (explicit vagy implicit módon) matematikai statisztikai elemet is tartalmaz, akkor olyan becslési módszert célszerű alkalmazni, amely eloszlástípusok széles spektrumára nagy hatásfokú. A tanulmány az általánosított leggyakoribb értékeket mutatja be ebből a szempontból.

ВОПРОСЫ ПОВЫШЕНИЯ ЭФФЕКТИВНОСТИ ГЕОФИЗИЧЕСКОЙ ИНТЕРПРЕТАЦИИ

Ференц ШТЕЙНЕР

Все увеличивающийся объем геофизических данных, поступающих вследствие полевых измерений, заставляет искать пути повышения эффективности извлечения информации, содержащейся в этих данных. Если альгоритм, используемый в интерпретации, содержит элементы математической статистики (в явной или неявной части уравнения), то целесообразно применение такого способа оценки, который обладает высокой эффективностью в широком диапазоне типов распределений. В статье представлены наиболее часто применяемые значения, важные для обсуждаемой проблемы.

GEOPHYSICAL TRANSACTIONS 1987
Vol. 33. No. 1. pp. 11–22

INTEGRAL IMPLEMENTATION OF DIP MOVEOUT

S. M. DERĘGOWSKI*

A relatively fast and accurate integral implementation of Dip Moveout is described and illustrated with examples using synthetic data. A proposed extension to arbitrary velocity variations is given.

Keywords: dip-moveout, velocity, common-depth-point method, signal-to-noise ratio, migration

1. Introduction

Dip Moveout transforms the data set so that each common midpoint gather actually contains events from the same depth point regardless of the dip of reflectors, and is capable of correction to a zero-offset trace by means of a simple hyperbolic NMO. For a complex overburden such a transformation requires knowledge of the depth model. But it turns out, somewhat surprisingly, that first order Dip Moveout is not only structurally independent but is also virtually velocity independent. That is, to a very good approximation, all the required information is contained within the arrival times, the time dips and the shooting geometry.

Dip Moveout started life in the mid seventies as Sherwood's DEVILISH [JUDSON, JIN LIN, SCHULTZ, SHERWOOD 1979]. This being an acronym for Dipping Event Velocity Inequality LIcked by SHerwood. Unfortunately the performance of the original DEVILISH was inadequate and the process "gave up" for quite small dips and offsets. DEVILISH was followed by a whole series of algorithms. YILMAZ and CLAERBOUT [1980] worked on another downward continuation technique which they termed Partial Prestack Migration. This name emphasizes the fact that Dip Moveout may be extracted as a separate operation from the full prestack time migration operator but obscures the fact that Dip Moveout is a full migration to zero offset. But this algorithm also failed to work satisfactorily, particularly at early times. The work at Stanford University provided the inspiration for a theoretical paper by DERĘGOWSKI and ROCCA [1981] from which the integral method described here has been extracted. BOLONDI, LOINGER and ROCCA [1982] subsequently provided an alternative finite difference approach, termed Offset Continuation. A Fourier transform implementation was taken up by HALE [1984] at Stanford University who also

* The British Petroleum Company, Britannic House, Moor Lane, London EC2, England
Paper presented at the 47th meeting of the EAEG, 4–7 June, 1985, Budapest, Hungary

termed the algorithm Dip Moveout or DMO. HALE's ideas have been implemented by several contractors and result in accurate if expensive algorithms. The integral or Kirchoff style operator, described here, is also a strong contender. It is relatively fast and also reasonably accurate. The integral method also has the advantage of being extendible to quite severe lateral velocity variations.

2. Dip Moveout claims

We will list the claims for Dip Moveout that have led to all this interest. These claims are only completely fulfilled in constant velocity but the process is robust enough to afford substantial improvements in each respect even when velocity varies. A perfect Dip Moveout operator would:

1. Migrate each trace to zero offset so that the stacked section becomes a zero-offset section.
2. This in turn implies that post DMO, but prestack, common-midpoint gathers would actually contain common-depth-points as defined by normal incidence rays. That is, reflector point dispersal is removed.
3. Because zero-offset sections are now being tied to zero-offset sections, cross-line ties are improved.
4. Dead traces are interpolated automatically according to local time dips.
5. Coherent noise with impossibly steep dip is removed, but at the same time steeply dipping fault planes are better imaged.
6. The signal-to-noise ratio is improved, especially at high offsets.
7. Stacking velocities become dip independent.
8. Velocity analysis improves and provides velocities which are more appropriate for migration as well as stacking.
9. Diffractions are preserved ready for improved definition after migration.
10. Post stack time migration becomes equivalent to prestack time migration but at considerably less expense.

The extent to which these claims are fulfilled is adversely affected by rapid velocity variations. But DMO has a wide range of applications and at worst it reduces to an offset adaptive dip filter which removes steeply dipping noise without incurring the risk of leaving spurious alignments of random noise. Examples of the power of DMO are given elsewhere [DERĘGOWSKI 1986].

3. The integral operator

The required impulse response is shown in *Fig. 1*. The output CMP, or CDP location, runs horizontally whilst the vertical axis represents the output zero-offset time. The Dip Moveout impulse response is a lower portion of a semi ellipse whose horizontal axis coincides with zero time and has a full width equal to the offset. The DMO ellipse bottoms at the NMO corrected time. The impulse response runs up the sides of the ellipse to the points where the tangents reach

a maximum time dip corresponding to real dips of 90-degrees. The success of Dip Moveout in removing reflector point dispersal depends on getting the lateral shift as a function of time dip correct. Fortunately the lateral shift applied by Dip Moveout is fairly insensitive to errors in the NMO time shift. This allows us to delay accurate velocity analysis until after Dip Moveout has been applied, when it also becomes easier to do.

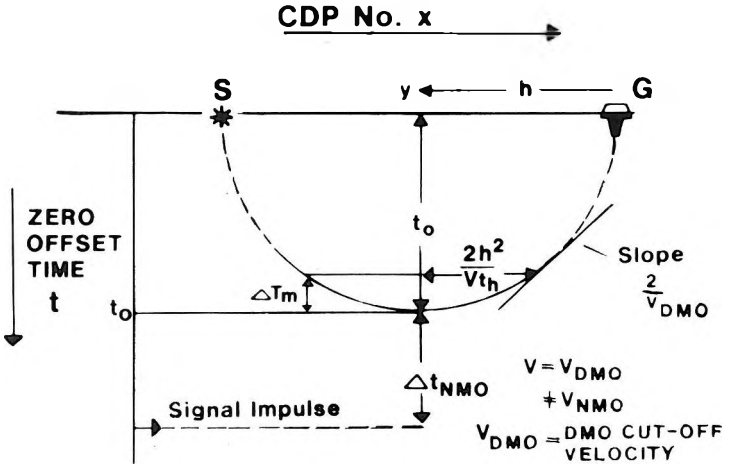

t_o = NMO corrected time

$t_h^2 = t_o^2 + 4h^2/V^2_{DMO}$

$x_m = 2h^2/V_{DMO}\, t_h$

$\triangle T_m = \left[1 - (1 - x^2_m/h^2)^{1/2}\right] t_o$

Fig. 1. Dip-moveout „smile" impulse response

1. ábra. A „dip-moveout" eljárás impulzus válaszfüggvénye

Рис. 1. Функция ответного импульса в способе поправки за наклон.

Because the Dip Moveout operator is migrating from a common-offset time section to a zero-offset time section it has a very important property not shared by other migration operators: when we migrate from time events to depth events the theoretical dip range is increased. That is: a direct time-to-depth conversion performed on a stacked section can at most produce 45-degree dips but these become 90-degree dips after migration. The maximum time dip output by standard migration operators is therefore limited by grid aliasing and cost. But when applying DMO to migrate to zero offset we know that for a constant velocity medium the maximum observable time gradient would be twice the reciprocal velocity. As shown by DERĘGOWSKI and ROCCA [1981] this

allows us to introduce automatic aperture control to the Dip Moveout operator according to something we can call a DMO cut-off velocity. That is, if S is the DMO impulse response whose amplitude and phase variation are contained in the time variant wavelet, L, then:

$$\begin{aligned} S(x, t, t_0) &= L(x, t, t_0) * \delta(t - t_0(1 - x^2/h^2)^{1/2}) \quad \text{if} \quad |x| \leq x_m \\ &= 0 \quad \text{if} \quad |x| \geq x_m \end{aligned} \tag{1}$$

where $x_m = 2h^2/(V_{DMO} t_h)$ and $t_h^2 = t_0^2 + 4h^2/V_{DMO}^2$.

It should be noted that the DMO cut-off velocity, V_{DMO}, has no direct relationship to the NMO velocity. In practice we normally set the DMO velocity constant and default it to 2000 m/s. It has the very important property that noise events, with impossibly steep time dips, are automatically dispersed. This has a significant effect in areas plagued by steeply dipping coherent noise. A further important property of Dip Moveout not shared by other 2-D migration operators is that it does not require the seismic line to be a dip line. It does however require the shot and receiver azimuths to be along the seismic line and hence is upset, for example, by large marine feathering angles.

Figure 2 shows some actual impulse responses produced by our integral type algorithm. The synthetic section shown is a stacked section. The prestack data set was all zero except for certain offsets of a few CMPs. These offsets are 900 m for CMP 10, 1000 m for CMP 50, 1500 m for CMP 110 and 2000 m at CMP 190. The Dip Moveout operator's amplitude and phase variation are also illustrated. Although not obvious from the figure the phase changes in a time variant manner from 45-degrees at high offsets to zero at very small offsets. This time variation has been obtained by windowing the half differential operator [Deregowski and Brown 1983, equations 17, 18] according to a triangular or Bartlett window whose length is determined by the depth of the impulse response:

$$L(x, t, t_0) = a(x) f(t, t_0) \tag{2}$$

$$f(t, t_0) = B(t, t_0) \cdot D_{1/2}(-t) \tag{3}$$

where

$$\begin{aligned} B(t, t_0) &= 1 - (t_0 - t)/\Delta T_m \quad \text{if} \quad t_0 - \Delta T_m \leq t \leq t_0 \\ &= 0 \quad \text{otherwise} \end{aligned}$$

and

$$D_{1/2}(t) = \frac{1}{\sqrt{\pi}} \frac{\delta(t)}{\sqrt{|t|}} - \frac{1}{2} \frac{H(t)}{|t|^{3/2}} \tag{4}$$

However what will be obvious to Dip Moveout experts is that, in this implementation, the amplitudes do not increase along the impulse response, at high offsets and small travel times, as required by the constant velocity wave equation. This is because these wave equation effects have been considered of secondary importance and have been omitted from the weighting function of the integral operator. Their introduction would increase the run time by about

five per cent. The weighting function is instead defined according to the cut-off velocity and follows the quadratic form suggested by DERĘGOWSKI and ROCCA [1981]:

$$a(x) = \frac{Vt_0}{2h^2}(1 - Ax^2)$$

$$= a_1 - a_2 x^2$$

But rather than using the various seismic parameters in its definition we simply require that the amplitude goes to zero at the maximum time slope, as defined by the cut-off velocity, in order to obtain a weighting function of the form:

$$a(x) = \frac{1}{\sqrt{x_m}}(1 - x^2/x_m^2) \tag{5}$$

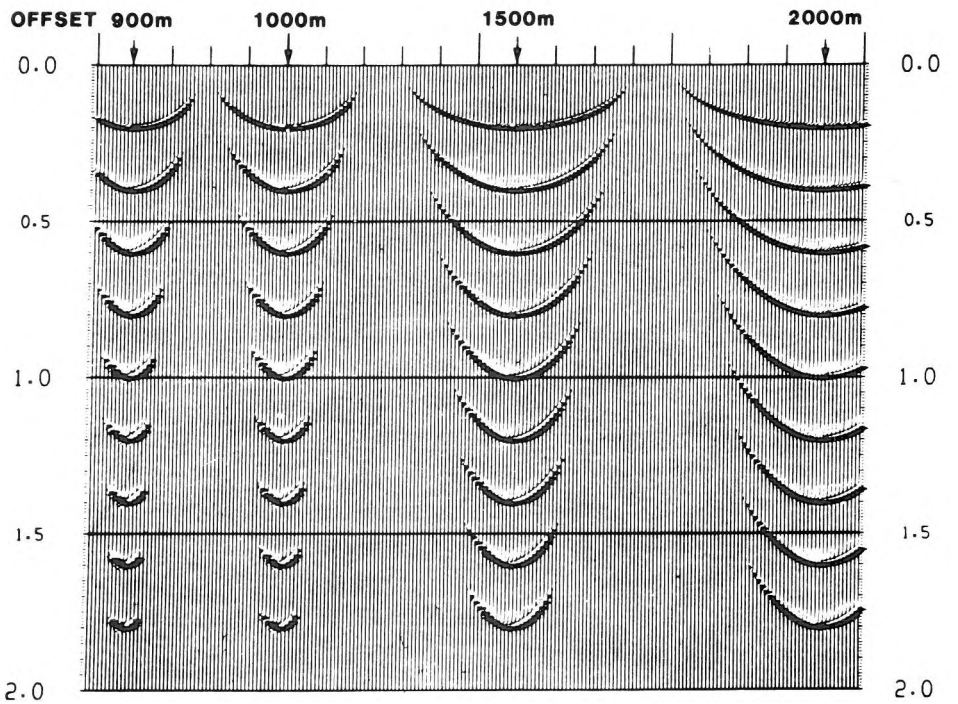

Fig. 2. Impulse responses at different offsets

2. ábra. Különböző robbantópont–geofon távolsághoz tartozó impulzus válaszfüggvények

Рис. 2. Функции ответных импульсов при различных расстояниях между взрывпунктом и сейсмоприемником.

The above equation may be regarded as the small offset approximation of the previous one. It has the numerical advantage of being directly determined by the aperture, x_m, of the DMO operator. The above equations (1)–(5) effectively define the integral $X-T$ algorithm we are using. In practice it is not necessary to sort the input data into common-offset subsets. *Figure 3* shows the data flow to an implementation which works from CMP-ordered data, and outputs results in the same order. Other forms of gather can equally well be accommodated.

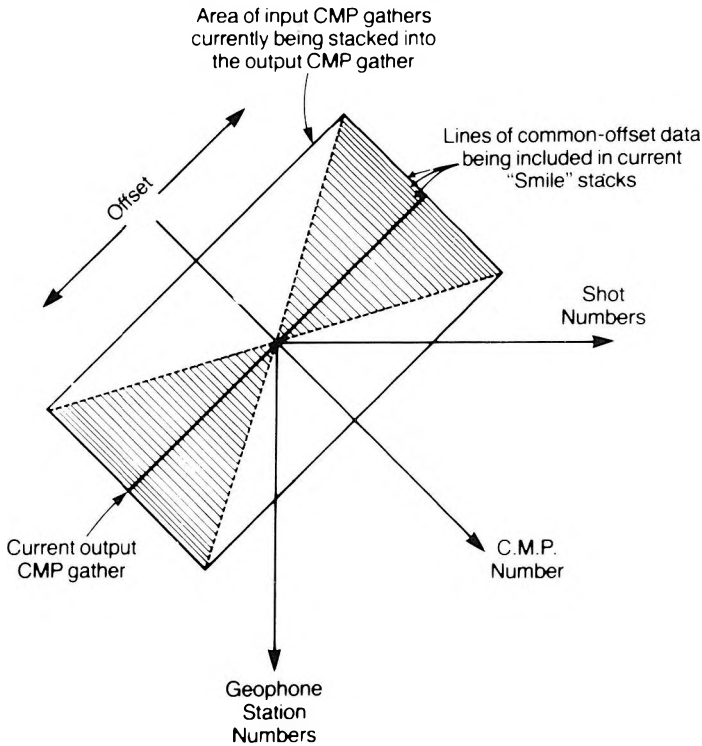

Fig. 3. Data flow in the algorithm

3. ábra. Adatáramlás az algoritmusban

Рис. 3. Перемещение данных в альгоритме.

Cost is directly proportional to the extent of coverage and the mean aperture, and is inversely proportional to the time sampling interval. One way of reducing cost is to reduce the number of offset planes by partial stacking. This, however, requires knowledge of reasonably accurate velocities and in regions of steep dip the NMO function used for DMO should differ from that required for stacking. Also at high offsets the DMO operator is too offset-dependent for this scheme to maintain accuracy. Consequently we almost always image all offset planes individually. The second way to cut cost is to increase the time sampling interval. The advantage here is that if we ignore the

implied high frequency loss then the algorithm becomes less dispersive for steep dips and coarse CMP spacing. In practice this means that data with a coarse CMP spacing are resampled. Thus 2 ms time sampling would only be used for a 10 m CMP spacing, and for a 25 m trace spacing a 6 ms interval is often used. Finally we could increase the dip limiting velocity as this directly affects the mean aperture. Doubling the DMO cut-off velocity halves the run time. But note that if the dip limiting velocity is set to twice the RMS then we end up with a 30-degree algorithm rather than a 90-degree one. There is, therefore, a significant danger of losing real steep events if the DMO cut-off velocity is increased much above the 2000 m/s default.

4. Reflector point dispersal

We will now have a closer look at reflector point dispersal. *Figure 4* shows the reflection geometry for a given shot and geophone location. The zero-offset travel path corresponds to the normal incidence ray; h is the half offset and ΔL is a measure of the reflector point dispersal. We see that if the surface midpoint is kept constant and the offset increased then the reflection point climbs up-dip by a distance proportional to the square of the offset and inversely proportional to the zero-offset time.

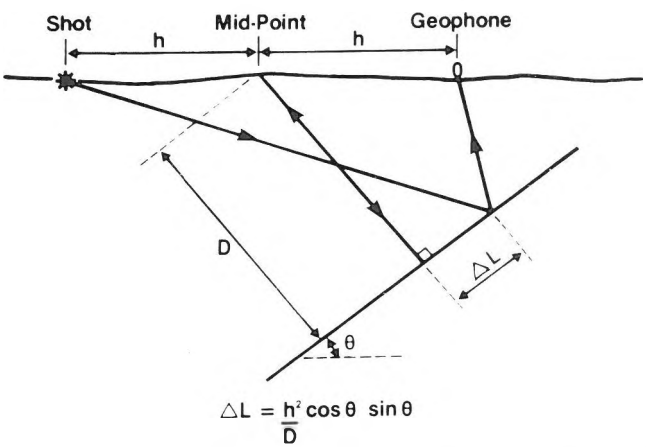

Fig. 4. Reflector point smear or dispersal, at a given CMP, as a function of dip and offset

4. ábra. A reflektáló pont diszperziója egy adott közös középpontra, a dőlés és a robbantópont–geofon távolság függvényében

Рис. 4. Дисперсия отражающей точки в заданном общем центре в зависимости от падения слоев и от расстояния между взрывпунктом и сейсмоприемником.

Figure 5 shows a stack over a synthetic data set without Dip Moveout. This data set was produced by simple raytracing over a constant velocity–depth model. The smallest offset in this 12-fold data set was set rather high at 1925 m

and the largest was 2500 m. The stacking velocity was set equal to the constant velocity of the medium and hence is only correct for the horizontal events. The raytracing failed to pick up a couple of reflections at CDP 438. This is fortunate as the same data served to illustrate the interpolative properties of Dip Moveout. It is noticeable that the dipping events become progressively more affected by reflector point dispersal and mis-stack as they become shallower.

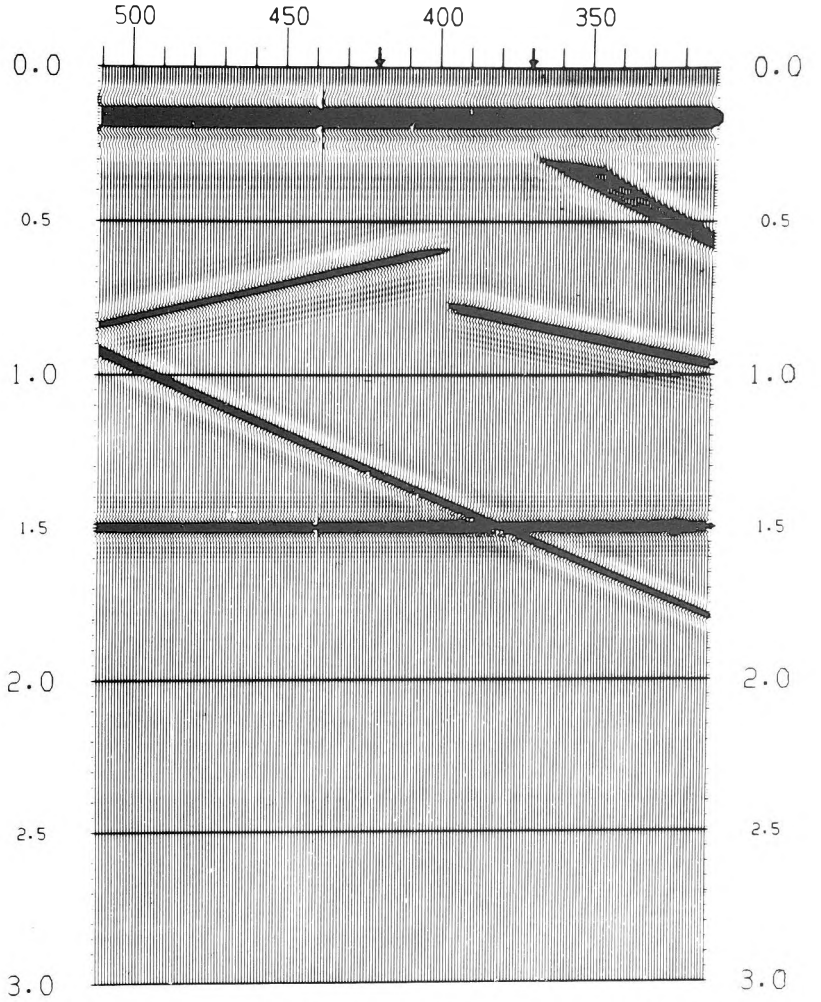

Fig. 5. 12-fold synthetic data stacked without DMO. Offset range: 1925 m–2500 m, trace spacing: 12.5 m, time sampling: 4 ms

5. ábra. 12-szeres fedésű szintetikus szelvény DMO nélkül. Robbantópont–geofon távolság: 1925 m–2500 m, geofonköz: 12.5 m, mintavételi köz: 4 ms

Рис. 5. Синтетический профиль с 12-кратным перекрытием без DMO. Расстояние между взрывпунктом и сейсмоприемником: 1925 м–2500 м, между сейсмоприемниками: 12,5 м, интервал отсчетов: 4 мс.

The left-hand arrow at the top of the section shows where the normal incidence reflection from the shallow dipping reflector should terminate. Because of the large inner offset its reflector point is dispersed so that the energy first appears in the CMP gather down-dip at the right-hand arrow.

Figure 6 shows the same data set, but stacked after Dip Moveout. It is pointed out that the relatively large migration distance of 625 m for the upper

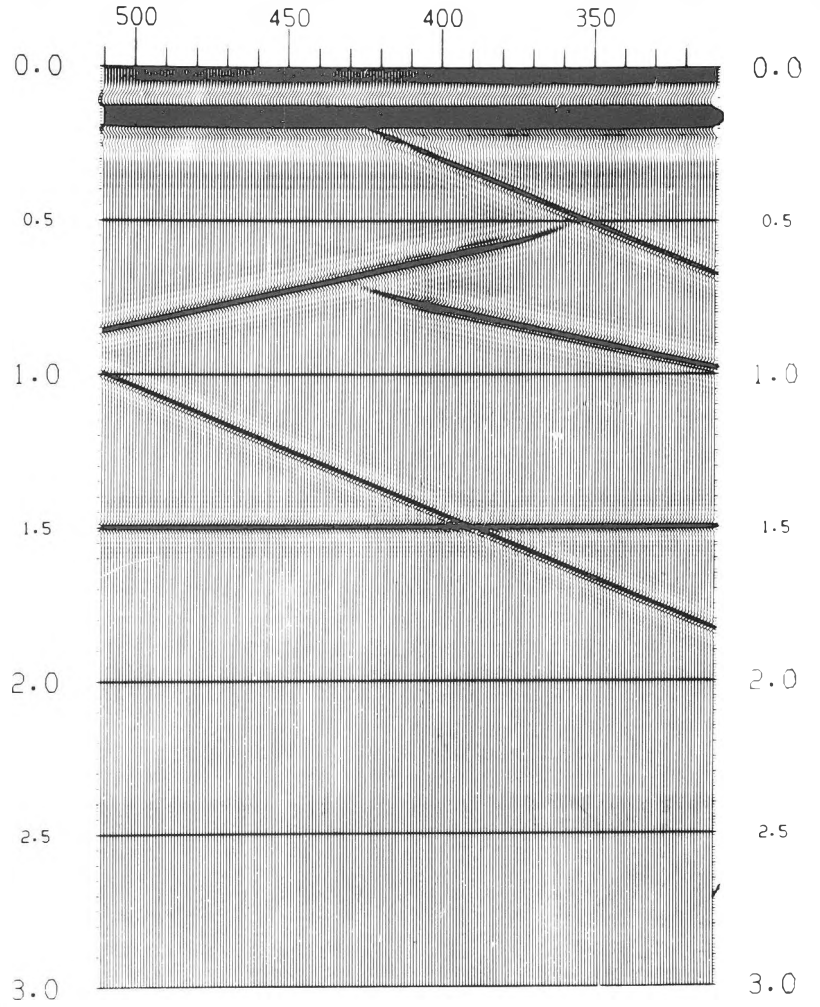

Fig. 6. 12-fold synthetic data stacked with DMO. Offset range: 1925 m–2500 m, trace spacing: 12.5 m, time sampling: 4 ms

6. ábra. 12-szeres fedésű szintetikus szelvény DMO-val. A modell paraméterek azonosak az 5. ábráéval

Рис. 6. Синтетический профиль с 12-кратным перекрытием с DMO. Параметры те же, что и на рис. 5.

termination point of the shallow dipping event has been correctly imaged to zero offset. This is the extent of the reflector point dispersal which would have been seen on the previous figure had the low offsets been included. The shallow, steeply dipping event is now well stacked. Also notable is the fact that the missing events have been interpolated.

5. Extension to complex overburdens

It has been mentioned that Dip Moveout is adversely affected by rapid velocity variations. Noise reduction apart, Dip Moveout benefits us by reducing reflector point dispersal [DERĘGOWSKI 1982]. Reflector point dispersal is, however, only completely removed in constant velocity. The first sign that all is not well is that, although the velocity analysis is still easier to pick, the stacked result shows little if any real improvement in resolution over the original stack. The final breakdown occurs when the velocity analysis also shows no benefit and we simply lose any steeply dipping coherent noise. That is, when the Dip Moveout operator degenerates into a prestack dip limiting filter. As shown in *Fig. 7* one solution is to ensure that Dip Moveout removes reflector point dispersal for a particular dip and overburden, by raytracing through an assumed velocity–depth model. The procedure is to find the reflection point, within the velocity–depth model, for the given offset, CMP and reflector. A normal incidence ray is then traced from the reflection point to the datum surface. This normal incidence ray gives us the required output time, t, the zero offset time dip, M, and the required DMO migration distance, Δy. The impulse response of the DMO operator is now distorted in order to remove completely the measured reflector point dispersal for the assumed dip, Θ.

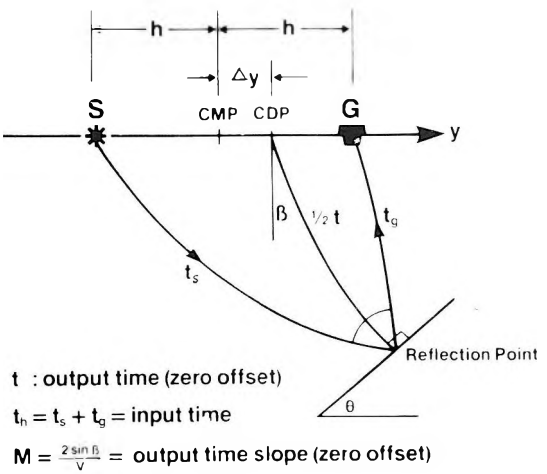

Fig. 7. Raytrace definition of DMO

7. ábra. A DMO eljárás sugárvezetéses definíciója

Рис. 7. Определение способа DMO через лучевую проводимость.

Figure 8 shows the proposed distortion of the DMO ellipse. We stretch the horizontal axis by the factor, γ, required to produce the correct migration shift,

Δy, in order te remove reflector point dispersal, but we also need to converse the required time dip, M, at the zero offset output time, t. To control both of these variables simultaneously we need another independent variable we can set. This is found in the NMO correction applied before the DMO operator. The normal moveout correction determines the timing, t_0, of the bottom of the dip-moveout ellipse. Instead of being determined by a stacking velocity this correction, together with the factor, γ, are now computed simultaneously according to the ray trace modelled time slope, M, and the required migration distance, Δy. That is, the pre-DMO NMO is also determined by raytracing through the assumed velocity–depth model. As I hope to demonstrate in a future paper, by using a raytrace defined stretch factor combined with a raytrace defined NMO, we can greatly enhance the removal of reflector point dispersal for specific events and still retain most of the other benefits of the constant velocity operator.

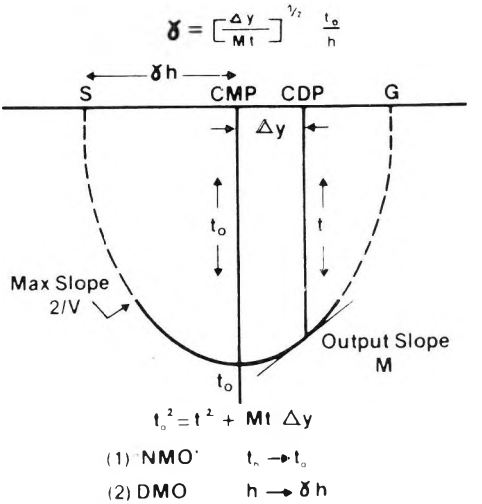

Fig. 8. DMO ellipse distorted by stretching the horizontal axis according to raytraced results. The stretch factor is time and space variant and can become pure imaginary

8. ábra. DMO ellipszis, a sugárútvezetési eredményeknek megfelelő horizontális nyújtással. A nyújtási faktor időben és térben változik és teljesen képzetessé is válhat

Рис. 8. Эллипс DMO, растянутый по горизонтали в соответствии с результатами лучевой проводимости. Фактор растяжения меняется как в пространстве, так и во времени, и может стать мнимой величиной.

6. Conclusions

DMO is a ubiquitous extension of CMP stacking affording many benefits. Of a number of methods of implementation, the integral in $X-T$ space as explained here, is the most direct, easly understood and controllable in its effects such as the maximum time dip retained. It is also efficient in that data traces

do not need to be resorted but can be handled in and out in any required order. One processing advantage of the standard operator is that it requires minimal control parameter selection. Apart from getting the shooting geometry right we need merely specify an approximate average NMO function. It should also be possible to extend dip-moveout theory in order to produce improved CDP stacks for quite complex overburdens. This should allow us to produce useful images in areas which might otherwise require full prestack depth migrations but at a fraction of the cost.

Akcnowledgements

I wish to express my gratitude to the Chairman and the Board of Directors of the British Petroleum Company for permission to publish this paper and to MR. J. W. J. Hosken for his critical and useful discussion.

REFERENCES

Bolondi G., Loinger E., Rocca F. 1982: Offset continuation of seismic sections. Geophys. Prosp. **30,** 6, pp. 813–828

Deręgowski S. M., Rocca F. 1981: Geometrical optics and wave theory of constant offset sections in layered media. Geophys. Prosp. **29,** 3, pp. 374–406

Deręgowski S. M. 1982: Dip-moveout and reflector point dispersal. Geophys. Prosp. **30,** 3, pp. 318–322

Deręgowski S. M., Brown S. M. 1983: A theory of acoustic diffractors applied to 2–D models. Geophys. Prosp. **31,** 2, pp. 293–333

Deręgowski S. M. 1986: What is DMO? First Break, **4,** 7, pp. 7–24

Hale I. D. 1984: Dip-moveout by Fourier transform. Geophysics, **49,** 6, pp. 741–757

Judson D. R., Jin Lin, Schultz P. S., Sherwood J. W. C. 1978: Equalizing the stacking velocities of dipping events via Devilish. Presented at the 48th Annual International SEG Meeting in San Francisco; brochure published by Digicon Geophysical Corp.

Yilmaz Ö., Claerbout J. F. 1980: Prestack partial migration. Geophysics, **45,** 12, pp. 1753–1779

A DŐLÉSKORREKCIÓS (DMO) ELJÁRÁS MEGVALÓSÍTÁSA INTEGRÁL OPERÁTORRAL

S. M. DERĘGOWSKI

A cikk a „dip-moveout" eljárás viszonylag gyors és pontos, integrál operátorral történő megvalósítását írja le és mutatja be szintetikus adatokon. Tetszőleges sebességváltozások esetére megoldást javasol.

ПРИМЕНЕНИЕ СПОСОБА ПОПРАВКИ ЗА НАКЛОН (DMO) С ИНТЕГРАЛЬНЫМ ОПЕРАТОРОМ

С. М. ДЕРЕНГОВСКИ

В статье дается описание применения способа поправки за наклон с интегральным оператором, обеспечивающим сравнительно высокие скорость и точность, и представляются результаты, полученные на синтетических данных. Предлагается решение для произвольных изменений скоростей.

GEOPHYSICAL TRANSACTIONS 1987
Vol. 33. No. 1. pp. 23–39

APPLYING THREE-COMPONENT RECORDS IN WAVE FIELD SEPARATION

R. DAURES* and P. TARIEL*

In zero-offset Vertical Seismic Profiles, the wave field includes only upgoing and downgoing *P*-waves having only vertical (*Z*) components. When the source is offset, the wave field becomes complicated by the presence of converted *P*–*SV*-waves different from *P*-waves by their apparent velocity and their direction of polarization. Seismic is no longer scalar but vectorial, and therefore three-component records are needed.

On the first arrival, the hodograph gives the polarization direction of the *P*-wave. The polarization direction of *P*–*SV*-waves is estimated by assuming a two-to-one *P* to *S* velocity ratio. The combined use of a set of axis-changes related to the directions of polarization, and the *f*–*k* filtering associated with the apparent velocities allows the separation of the total wave field into the four following types: downgoing *P*-, upgoing *P*-, downgoing *P*–*SV*- and upgoing *P*–*SV*-waves.

Keywords: vertical seismic profiles, offset VSP, *P*-waves, *P*–*SV*-waves, velocity filtering, polarization, wave field separation

1. Introduction

This paper addresses three-component recording (*X*, *Y*, *Z*) in a borehole, assuming gently dipping sedimentation. In the case of zero-offset Vertical Seismic Profiles (VSPs), the *P*-wave emitted from the surface reaches the reflectors with normal incidence, which does not generate converted waves. The recording of the vertical (*Z*) component provides full knowledge of the *P*-wave field. There is only one polarization direction, this being vertical. Seismic is then scalar, and up- and downgoing *P*-waves are differentiated by their apparent velocities. Many separation algorithms have already been used.

When the source is offset, the wave field becomes more complex. The *P*-wave emitted from the surface reaches the reflectors with far from normal incidence, and converted waves are generated (*P*-reflected *SV* and *P*-transmitted *SV*). Several types of waves appear, and each type is characterized by its own polarization direction and its own apparent velocity. Seismic is no longer scalar but vectorial. Complete knowledge of the wave field now requires three-component recording.

The aim is to separate the different types of waves in the (*Z*, *T*) domain limited by the times of the first *P*-arrival and the first *S*-arrival. We will assume that there are only four significant types of waves:

* Compagnie Générale de Géophysique 91341 Massy, France
Paper presented at the 47th meeting of the EAEG, 4–7 June, 1985, Budapest, Hungary

— downgoing *P*
— upgoing *P*
— downgoing *P–SV* (*P*-waves converted to *SV* mode through transmission)
— upgoing *P–SV* (*P*-waves converted to *SV* mode through reflection).

On the first arrival, the hodograph gives the polarization direction of the *P*-wave. The polarization direction of *P–SV*-waves is estimated by assuming a two-to-one *P* to *S* velocity ratio.

The combined use of a set of axis-changes related to the directions of polarization, and the *f–k* filtering associated with the apparent velocities, allows the total wave field to be separated into the four following types: downgoing *P*-, upgoing *P*-, downgoing *P–SV*- and upgoing *P–SV*-waves.

There are four stages in this separation:

a) Vector composition of two horizontal components to represent the problem in 2-D.

b) Change in the set of axes according to the polarization direction of downgoing *P*-waves and to its orthogonal direction, with velocity filtering of the *P*-waves on the first component.

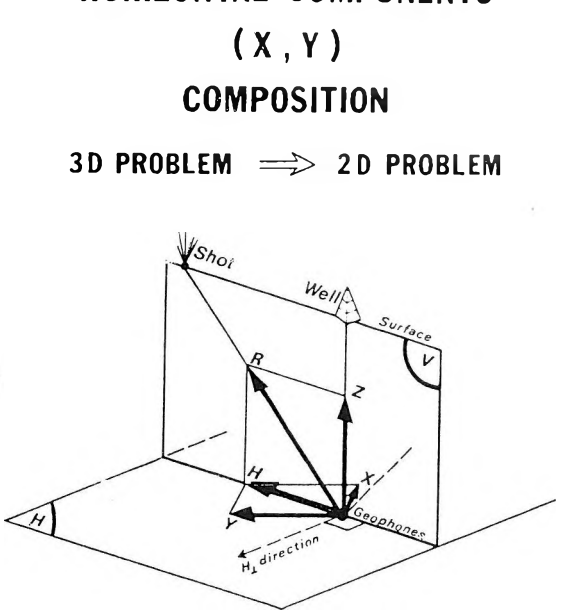

Fig. 1. Schematic diagram of detector orientation using three-component geophone in a VSP recording survey

1. ábra. Detektor orientáció háromkomponenses geofonnal készített VSP felvétel esetén

Рис. 1. Ориентировка детектора при записи ВСП с использованием трехкомпонентных сейсмоприемников.

c) Second change in the set of axes according to the polarization direction of downgoing *P–SV* waves and to its orthogonal direction, with velocity filtering of the *P–SV* waves on the first component.

d) Separation of upgoing *P*-waves and upgoing *P–SV*-waves by changing the set of reference axes.

Each type of wave usually shows projections on the three-component axes since the projection system is randomly oriented (see *Fig. 1*). The first operation consists of selecting a reference system with one vertical plane containing the source. We then face only a 2-D problem about the couple of components (*Z* and *H*) belonging to that plane *(Fig. 2)*. In order to perform this rotation, the two horizontal components of the initial system are conventionally added so as to maximize the energy of the direct wave. A very weak level of residual energy appears along the perpendicular *H* direction *(Fig. 3)*, which generally confirms the existence of a measurement plane containing most of the energy of the *P*- and *SV*-waves.

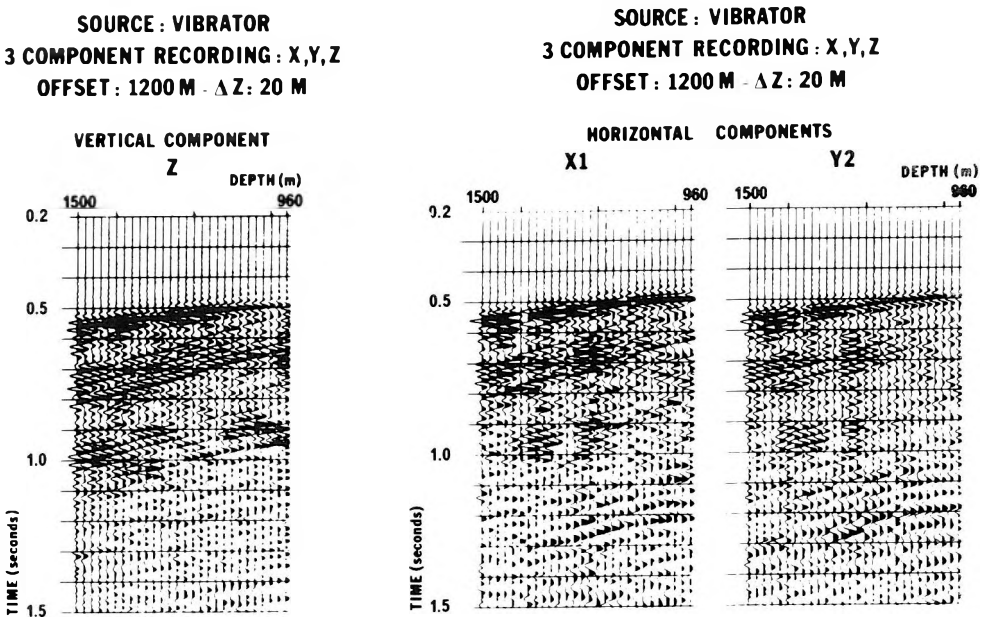

Fig. 2. Offset VSP raw data. Three-component well geophone recording: one vertical (left) and two horizontal (right) components

2. ábra. Távoli gerjesztésű VSP felvétel háromkomponensű lyukgeofonnal: egy függőleges (bal oldalon) és két vízszintes (jobb oldalon) komponens

Рис. 2. Запись ВСП с дальним возбуждением с использованием трехкомпонентных скважинных сейсмоприемников: одна компонента вертикальна (на левой стороне), а две другие горизонтальны (на правой стороне).

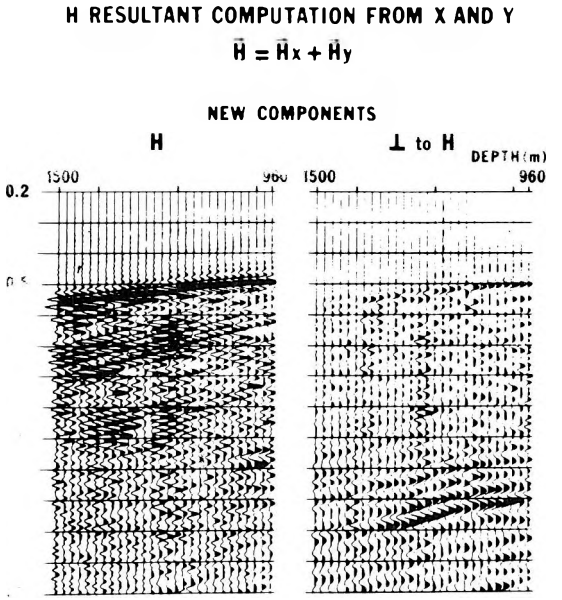

Fig. 3. Horizontal resultant (*H*) and its perpendicular component from hodograph derived on first *P*-arrival

3. ábra. Az elsődleges *P* beérkezésre meghatározott hodográfból számított vízszintes eredő (*H*) és az erre merőleges vízszintes komponens

Рис. 3. Горизонтальная результирующая (*H*), рассчитанная по годографу, выведенному для первичных вступлений продольных волн, и перпендикулярная к ней горизонтальная компонента.

2. Estimation of polarization directions

Using the Z and H components, it is easy to define the polarization direction of the direct *P*-arrival. First the time (t_1) of the direct travel path of the *P*-wave from source to receiver is picked.

Then the construction of a hodograph yields the angle AG between the polarization direction of the downgoing *P*-wave and the vertical *(Fig. 4.)* We may infer from the first *P*-arrival the sketch of the propagation directions of the four types of waves *(Fig. 5)* and the diagram of the polarization directions *(Fig. 6)*. Supposing that we have roughly $V_P = 2V_S$, the angle β of the direction of propagation of *S*-wave is given by:

$$\sin \beta = \frac{1}{2} \sin \alpha.$$

At time t_1, if α_1 is the polarization angle of the downgoing *P*-wave measured on the hodograph:

— the polarization angle of the upgoing P-wave is $(-\alpha_1)$
— the polarization angle of the converted downgoing P–SV is $(\pi/2+\beta_1)$
— the polarization angle of the converted upgoing P–SV is $(\pi/2-\beta_1)$

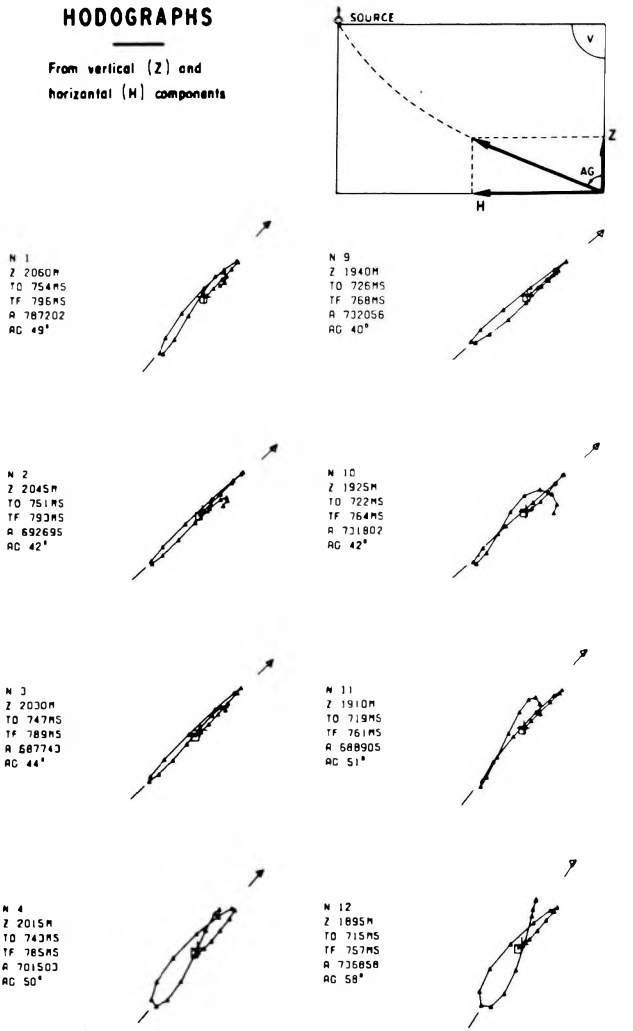

Fig. 4. Hodographs derived from Z and H components
Z — depth; *TO* — time of first break; *TF* — time of last sample; *AG* — angle of polarization

4. ábra. A Z és H komponensekből levezetett hodográfok
Z — mélység; *TO* — első beérkezés ideje; *TF* — utolsó mintavétel; *AG* — a polarizációs szög

Рис. 4. Годографы, выведенные из компонент Z и H
Z — глубина; *TO* — начальный момент времени; *TF* — конечный момент времени; *AG* — угол поляризации.

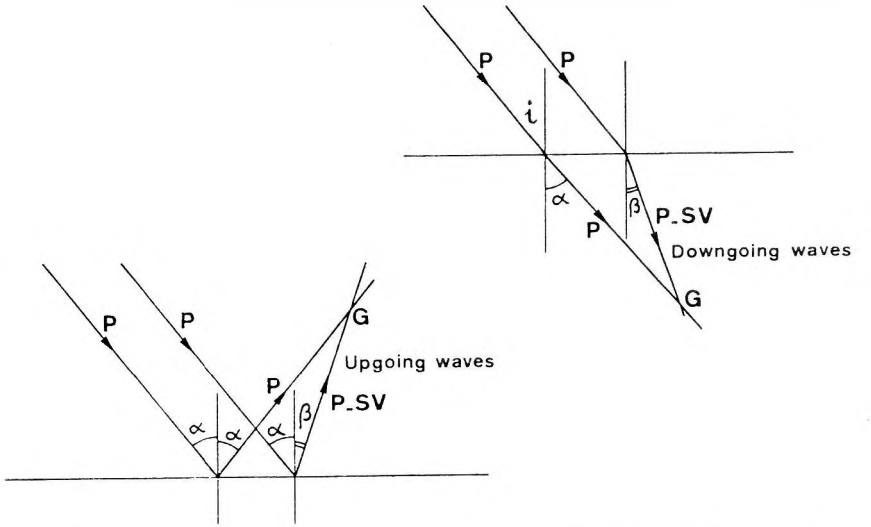

Fig. 5. Schematic of the ray paths close to the geophone for the four main types of waves. Downgoing waves: *P* and converted *SV*; upgoing waves *P* and *SV*

5. ábra. A geofonhoz közeli sugárutak vázlata a négy fő hullámtípusra. Lefelé haladó hullámok: *P* és konvertált *SV*; felfelé haladó hullámok: *P* és *SV*

Рис. 5. Схема лучевых путей вблизи от сейсмоприемника для четырех основных типов волн: нисходящих *P* и преобразованных *SV*, а также восходящих *P* и *SV*.

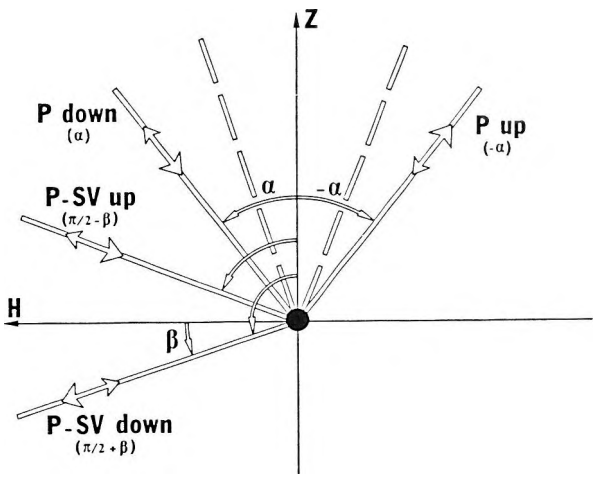

ASSUMPTION : $V_P/V_S = 2 \Rightarrow \sin\beta = 0.5 \sin\alpha$

Fig. 6. Directions of polarization relating to the wave modes close to the first *P*-arrivals

6. ábra. Polarizációs irányok az első *P* beérkezésekhez közeli hullámfajtákra

Рис. 6. Направления поляризации для волн, близких к первым вступлениям продольных волн.

Third, the polarization angles are estimated as a function of time. In the case of a constant velocity V_P (reflection coefficients are then derived from density variations), a simple relationship is found for both up- and downgoing *P*-waves:

$$\sin \alpha_i = \frac{t_1}{t_i} \sin \alpha_1$$

which yields the value of the polarization direction versus time. Simple formulae also lead to the estimation of polarization angles for *P–SV*-downwaves and *P–SV*-upwaves.

To be realistic, we chose a model with a given V_P velocity at the receiver level and a low varying average velocity from the surface, still with $V_P = 2V_S$. The estimates of the simplified model of constant velocity are still valid. The study was made with the following source offset to depth ratios: 0.25, 0.5, 1.0 and 1.5, and the following interval velocity (at geophone depth) to RMS velocity ratios: 0.5, 1.0, 1.5 and 2.0. *Figure 7* illustrates the raypaths with an equal distance for the source offset and the geophone depth; the velocity ratio is 1.5

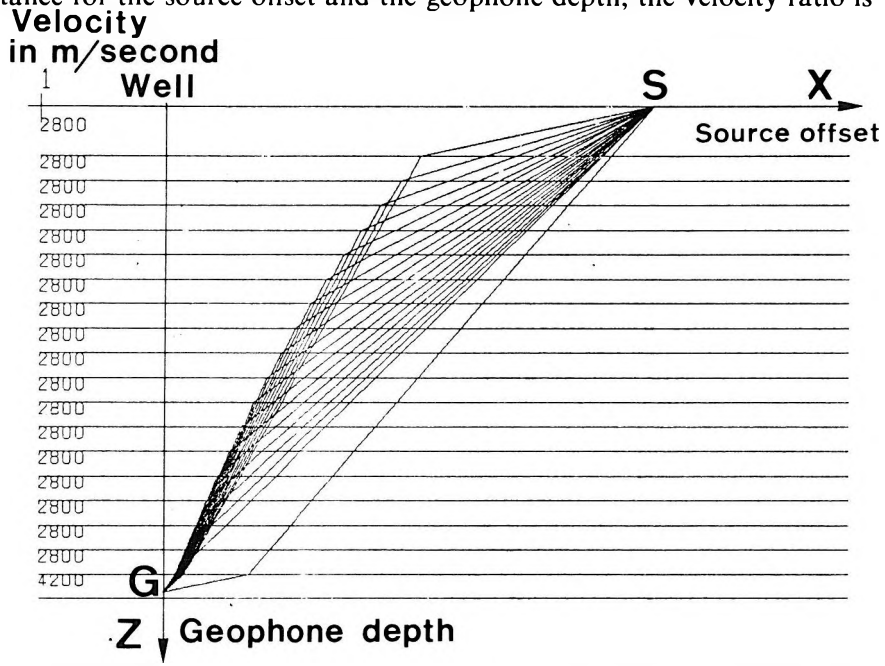

Fig. 7. Example of raytracing modelling for converted downgoing wave. Interval velocity at geophone depth is 4200 m/s, average velocity is 2800 m/s

7. ábra. A sugárkövetéses modellezés példája konvertált lefelé haladó hullámra. A geofon mélységében az intervallum sebesség 4200 m/s, az átlagsebesség 2800 m/s

Рис. 7. Пример моделирования путем прослеживания лучей для нисходящей преобразованной волны. На глубине сейсмоприемника интервальная скорость составляет 4200 м/с, а средняя скорость — 2800 м/с.

giving 4200 m/s for the interval velocity at the geophone and 2800 m/s for the average velocity. *Figure 8* shows the graph of the estimates of polarization directions plotted against time for the four types of waves.

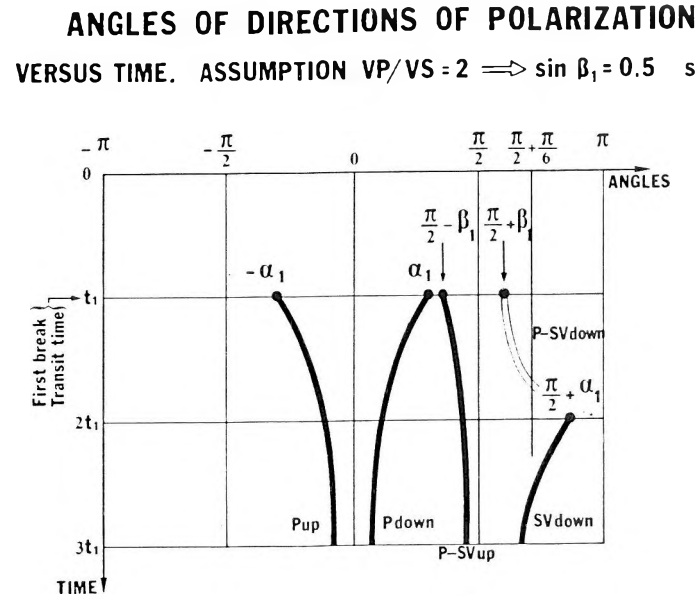

Fig. 8. Angles of wave polarization versus time for the different wave modes

8. ábra. Hullámpolarizációs szögek az idő függvényében, különböző hullámfajtákra

Рис. 8. Углы поляризации волн в зависимости от времени для различных типов волн.

3. Principle of wave separation

The coordinate system is changed so that a given type of wave is entirely determined by one of the components of the new system. The orthogonal component then only contains the projections of the other types of waves. For instance, from the fixed (Z, H) system of coordinates, we may choose the time variant system constituted by the P-downwave and its perpendicular direction. An f–k bandpass filter over the P down direction will provide the P down component. An f–k rejection filter over the same direction will provide two time-variant orthogonal components which only contain the other types of waves. We may then proceed with time-variant changes of coordinates and f–k filtering to isolate a new type of wave, and yield two other time-variant orthogonal components which will only contain two types of waves.

In practice, the most energetic downgoing P and downgoing P–SV events are progressively eliminated so as to recover two orthogonal components which only include upgoing P- and P–SV-waves. These waves are then separated by

a simple change of coordinates. The flowchart and the diagrams of the different systems of coordinates illustrate all the successive stages of the algorithm *(Fig. 9)*.

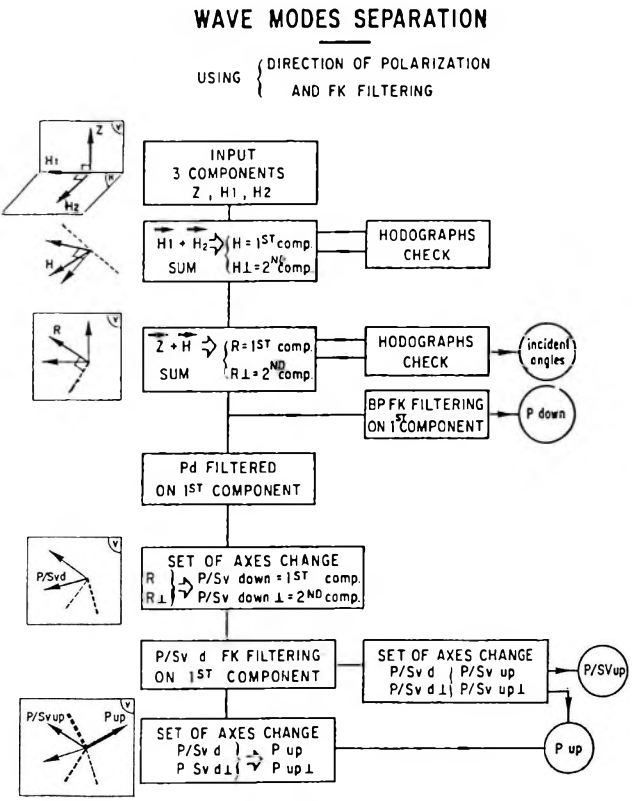

Fig. 9. Processing flowchart for wave field separation

9. ábra. A hullámtér szétválasztás folyamatábrája

Рис. 9. Схема процесса расчленения волнового поля.

4. Examples

The first example shows the wave field separation applied to offset VSP data. The downhole tool housed a three-component orthogonal geophone and the data were recorded from 1500 m to 960 m every 20 meters. A vibrator located at 1200 m from the wellhead was used as a seismic source.

First, hodographs are derived from a small window a few tens of milliseconds wide near the f rst *P*-arrival and the angle α of the polarization direction is calculated. This processing phase is important since the quality of the separation depends on the accuracy of determination of the angle α. It is very interesting to compare the angle values with the velocities derived from the sonic

log *(Fig. 10)*. Their validity can then be estimated, and questionable measurements can possibly be eliminated.

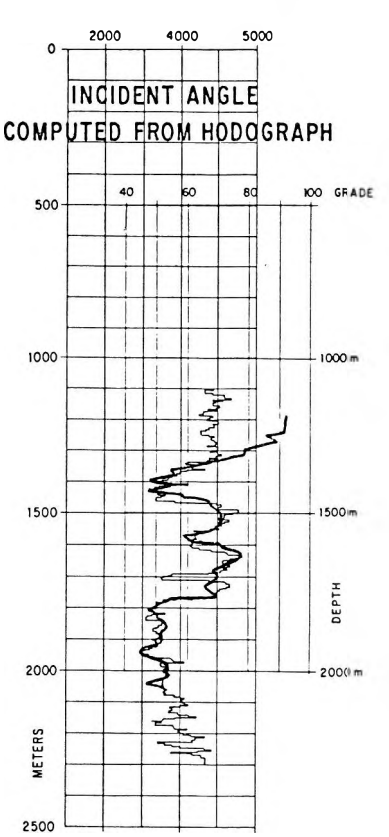

Fig. 10. Comparison of the incident angles (thick line) obtained from hodographs (Z and H components) with the sonic log velocity (thin line)

10. ábra. A hodográfból (Z és H komponens) számított beesési szögek (vastag vonal) összehasonlítása a szónikus intervallum sebességgel (vékony vonal)

Рис. 10. Сопоставление углов вхождения (жирная линия), рассчитанных по годографам (компонент Z и H), с акустической интервальной скоростью (тонкая линия).

The downgoing P- and P–SV-waves are separated after the process described above. The first change in coordinates is performed from the fixed (Z, H) system to the time-variant system constituted by the direction of the downgoing P-wave (R) and its perpendicular direction to facilitate rejection of the downgoing P-waves *(Fig. 11)*. The second change in coordinates is performed from the preceding system to the time-variant system constituted by the direction of polarization of the downgoing P–SV-wave and its perpendicular direction, to facilitate rejection of the downgoing P–SV-waves.

The results of the separation applied to the Z and H components *(Fig. 2)* are shown in *Figs. 12* and *13*. We notice in Fig. 13/b a residual downgoing P–SV-wave which is probably associated with elliptic polarization. Rejection on one component only is not sufficient in this case. Figure 13 is displayed with +9 dB gain to improve visibility.

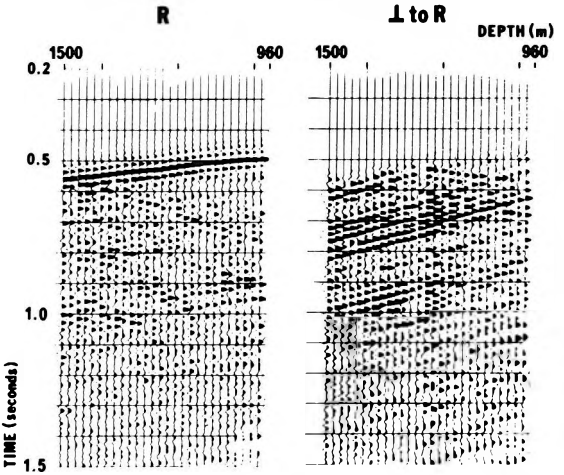

Fig. 11. New components after rotation of axes, polarized in the direction of the downgoing *P*-wave and its perpendicular component

11. ábra. A tengelyek elforgatásával keletkező új komponensek a lefelé haladó *P*-hullám irányába és az arra merőleges irányba polarizálva

Рис. 11. Новые компоненты, возникающие при повороте осей, поляризованные в направлении нисходящей продольной волны и перпендикулярно к ней.

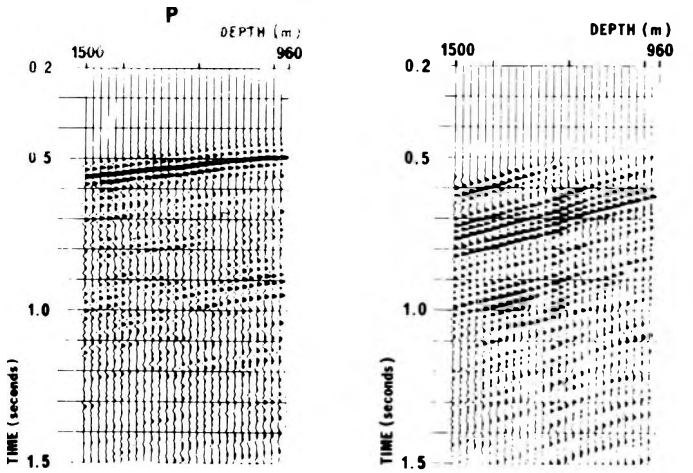

Fig. 12. Wavefield separation: downgoing *P*- (left) and *SV*-waves (right) after rotation of axes and *f–k* filtering

12. ábra. Hullámtér szétválasztás: lefelé haladó *P*- (bal oldalon) és *SV*-hullám (jobb oldalon) a tengelyek elforgatása és *f–k* szűrés után

Рис. 12. Расчленение волнового поля: нисходящие волны *P* (слева) и *SV* (справа) после поворота осей и *f–k* фильтрации.

Figures 14 to 16 illustrate the main steps of this method on another VSP data set with greater offset. The vibrator was located 1775 metres from the wellhead, and the geophone spacing was 30 meters from 2060 m to 1100 m.

Figure 14 shows the 3 components of the raw VSP data. We should note that for the shallowest geophones, the first *P*-arrivals can only be seen on the horizontal components (*H*1, *H*2) because of large angles of incidence. *Figures 15* and *16* show the results of the separation.

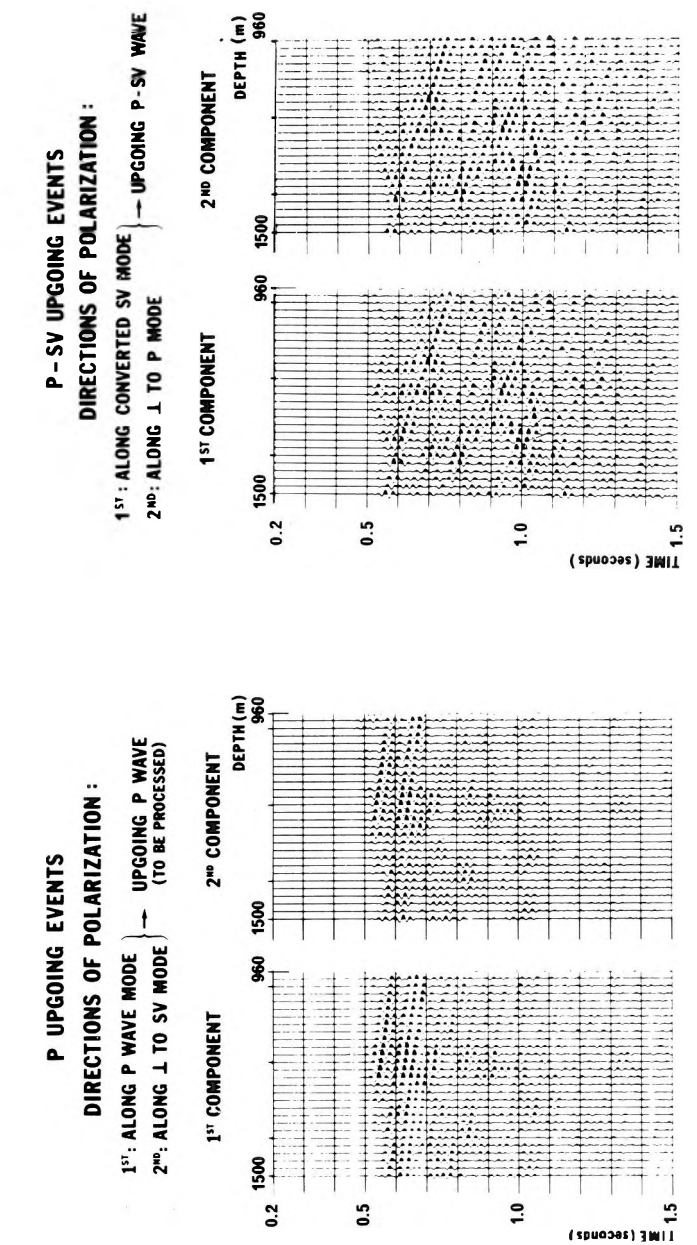

Fig. 13. Wave field separation: upgoing *P*-wave (left) and upgoing converted *SV*-waves (right)

13. ábra. Hullámtér szétválasztás: felfelé haladó *P*-hullám (bal oldalon) és konvertált *SV*-hullám (jobb oldalon)

Рис. 13. Расчленение волнового поля: восходящие волны *P* (слева) и преобразованные волны *SV* (справа).

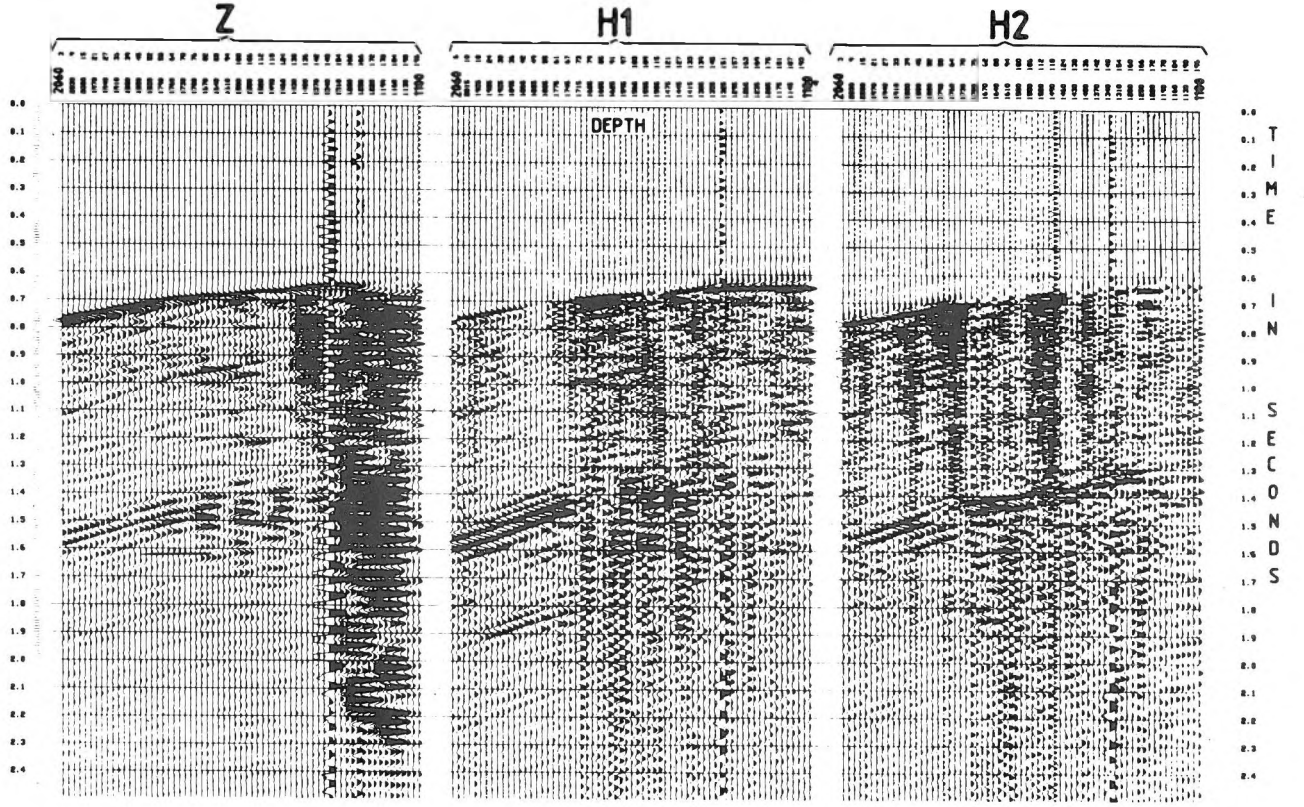

Fig. 14. Three-component VSP raw data: vertical and horizontal components. Geophone levels from 2060 m to 1100 m below KB. Vibrator 1775 m from wellhead, sweep 13–100 Hz

14. ábra. Háromkomponenses VSP felvételek: függőleges és viszintes komponensek. Geofon szintek 2060 m-től 1100 m-ig a forgatóasztal szintje alatt. A vibrátor a fúrás helyétől 1775 m távolságra volt, vibroje! 13–100 Hz

Рис. 14. Трехкомпонентные записи БСП вертикальные и горизонтальные компоненты. Уровни сейсмоприемников — с 2060 м до 1100 м под ротором. Вибратор находился в 1775 м от скважины, вибросеймический сигнал — с 13 гц до 100 гц.

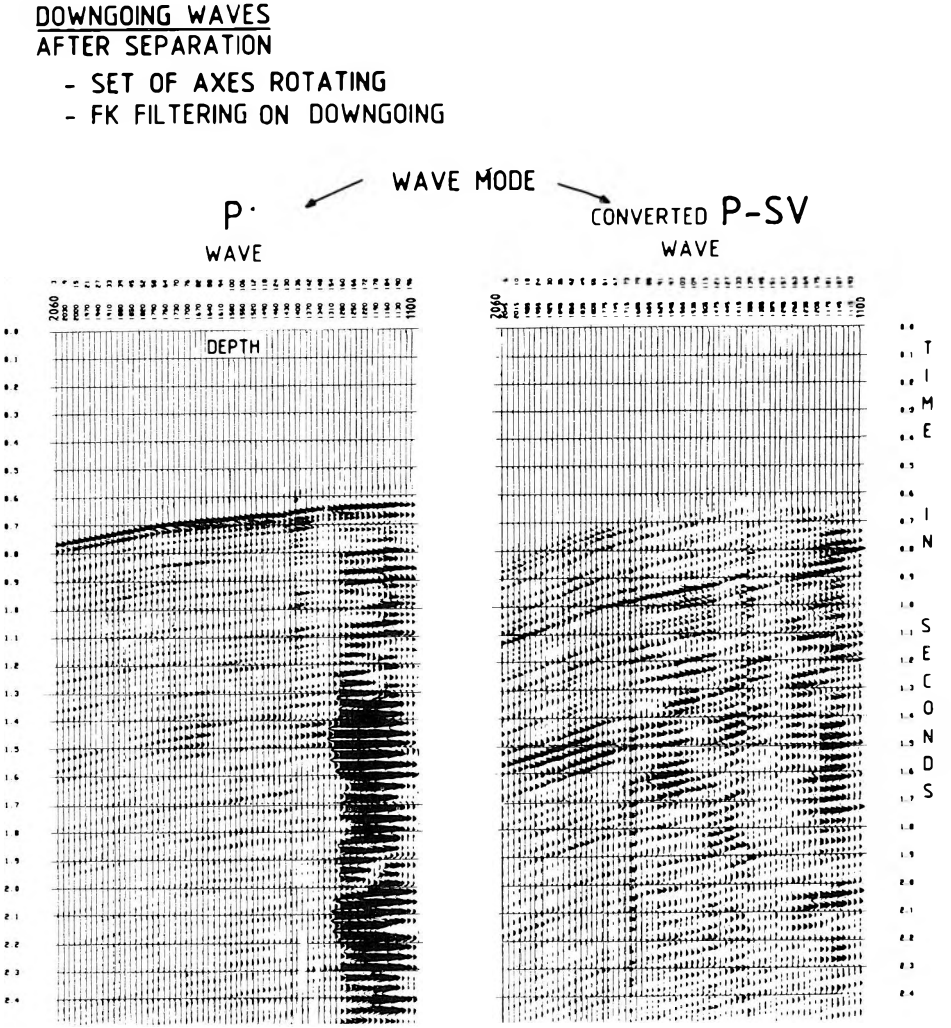

Fig. 15. Downgoing *P*- and converted *SV*-waves after time variant wave field separation: rotation of axes and *f–k* filtering

15. ábra. Lefelé haladó *P*- és konvertált *SV*-hullámok, időben változó hullámtér-szétválasztás után: tengelyek elforgatása és *f–k* szürés

Рис. 15. Нисходящие волны *P* и преобразованные волны *SV* после расчленения волнового поля с изменением во времени: поворот осей и *f–k* фильтрация.

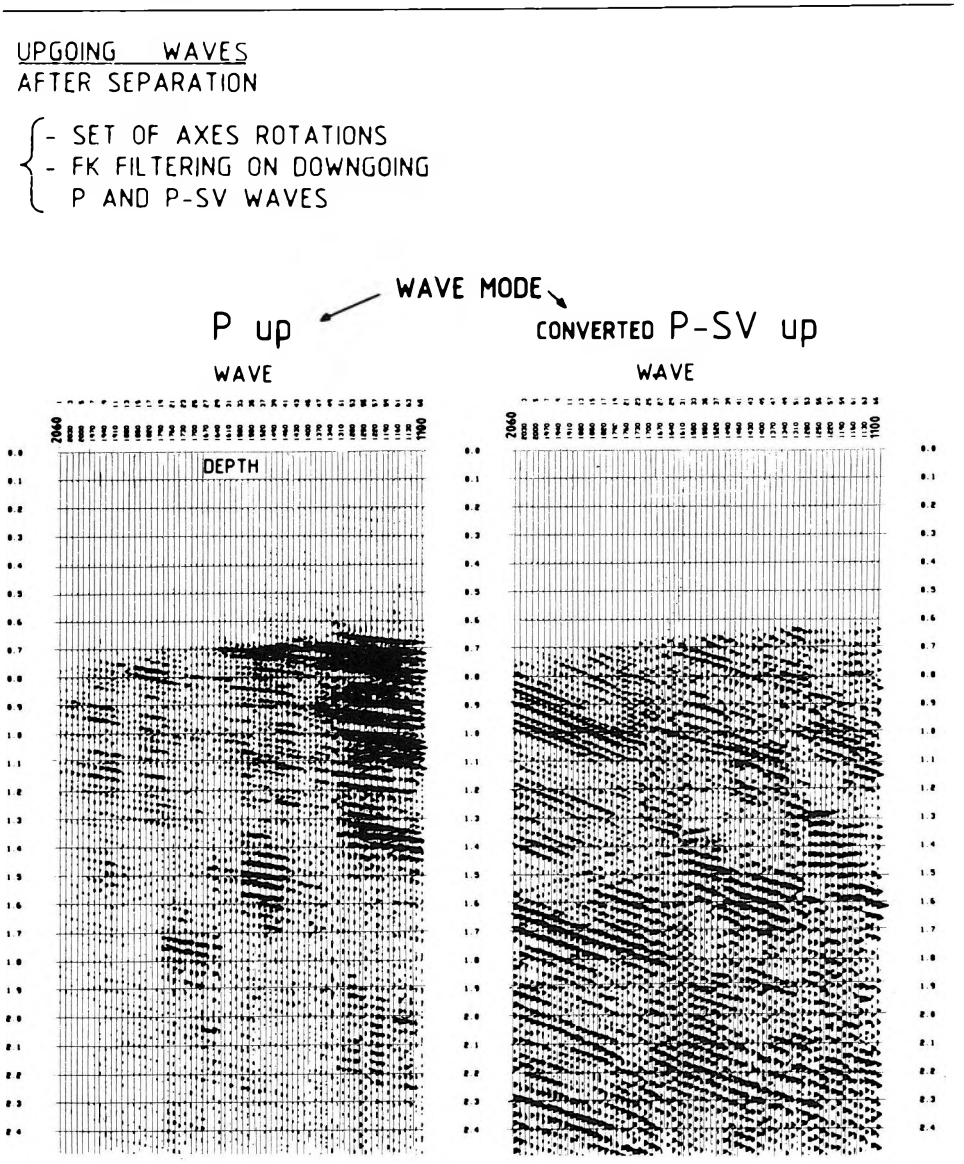

Fig. 16. Upgoing *P*- and converted *SV*-waves after time-variant wave field separation

16. ábra. Felfelé haladó *P*- és konvertált *SV*-hullámok, időben változó hullámtér-szétválasztás után

Рис. 16. Восходящие волны *P* и преобразованные волны *SV* после расчленения волнового поля с изменением во времени.

Comparison between two corridor stacks derived from zero-offset upgoing *P*-events and upgoing converted *SV*-events is illustrated in *Fig. 17*. *SV*-waves have been separated as stated above then plotted versus *P* traveltime by using the relationship between *P* and *S* times picked from zero-offset VSP data.

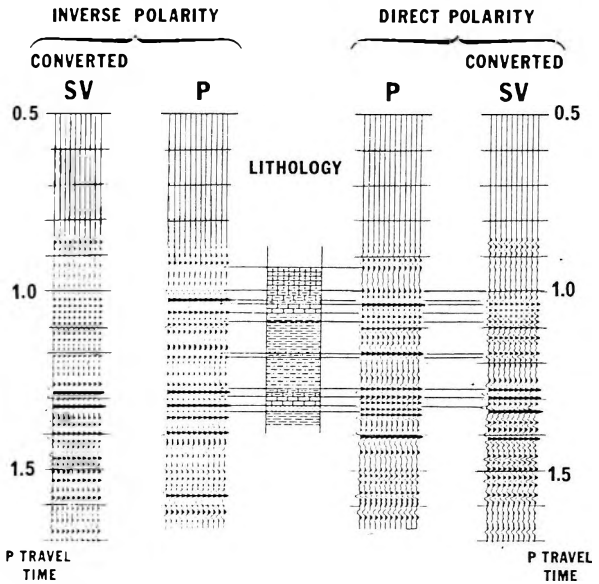

Fig. 17. Application of converted upgoing shear wave by comparison with upgoing *P*-waves with the same time-scale and related lithology

17. ábra. Konvertált felfelé haladó nyíró hullám alkalmazása felfelé haladó *P*-hullámokkal való összehasonlításra, azonos időlépték és a megfelelő rétegsor esetén

Рис. 17. Сопоставление преобразованных восходящих поперечных волн с восходящими продольными волнами в случае тождественных временных масштабов и подходящей литологической колонки.

5. Conclusion

The algorithms we have described proved efficient and robust in industrial applications as shown by many examples. The use of time-variant changes in coordinates seems to bring an improvement with respect to tests carried out with constant polarization angles plotted against time.

We may proceed separately for the processing of each type of wave. The wave field separation and the processing of the upgoing converted *SV*-waves up to the corridor stack provide a VSP log of *P–SV*-waves. This *P–SV* converted wave log is particularly interesting as the converted wave surface recording keeps developing and comparison between the "converted wave" section and

the *P–SV* converted wave log should facilitate overall interpretation. However, the main advantage is to improve the quality of later stages of the processing, in the case of Vertical Seismic Profiles with large offsets. We will summarize our experience as follows:

— for small offsets, seismic response is obtained from the *Z*-component only,
— for average offsets, the processing addresses the vertical component too, but the total wave (*R*) is used to find the downgoing signal that is useful for deconvolution,
— for large offsets, the energy of upgoing and downgoing *S*-waves becomes very great. Processing then demands more accurate separation as described above.

HÁROMKOMPONENSŰ FELVÉTELEK ALKALMAZÁSA HULLÁMTEREK SZÉTVÁLASZTÁSÁRA

R. DAURES és P. TARIEL

A lyukszáji gerjesztésű VSP méréseknél a hullámtér csak felfelé és lefelé haladó *P*-hullámokat tartalmaz, melyek csak vertikális (*Z*) komponensekből állnak. Ha a gerjesztés távolabb van, a hullámtér bonyolultabbá válik a konvertált *P–SV*-hullámok jelenléte miatt, melyek a *P*-hullámoktól eltérnek mind látszólagos sebességükben, mind polarizáltsági irányukban. A szeizmika ettől fogva nem skaláris, hanem vektoriális jellegű, és emiatt három komponensű felvételekre van szükség.

Az első beérkezésekre a hodográf megadja a *P*-hullám polarizációs irányát. A *P–SV*-hullámok polarizációs irányát 2:1 arányú *P–S* sebességhányados feltételezésével becsüljük. A tengelyeknek a polarizációs irányokhoz viszonyított változtatásai és a látszólagos sebességekhez kapcsolt *f–k* szűrés együttes alkalmazása lehetővé teszi a teljes hullámtér felosztását az alábbi négy hullámtípusra: lefelé haladó *P*, felfelé haladó *P*, lefelé haladó *P–SV*, és felfelé haladó *P–SV*-hullámok.

ПРИМЕНЕНИЕ ТРЕХКОМПОНЕНТНОЙ ЗАПИСИ В РАСЧЛЕНЕНИИ ВОЛНОВЫХ ПОЛЕЙ

Р. ДОР и П. ТАРЬЕЛ

При измерениях методом вертикального сейсмического профилирования (ВСП) с возбуждением волн на устье скважины волновое поле состоит исключительно из восходящих и нисходящих продольных волн, содержащих одни вертикальные компоненты (*Z*). При перемещении точки возбуждения на некоторое расстояние от скважины волновое поле становится более сложным в связи с появлением преобразованных *P–SV* волн, отличающихся от продольных (*P*) волн как в кажущейся средней скорости, так и в направлении поляризации. С этого момента сейсморазведка вместо скальярной становится векторной, поэтому возникает необходимость в трехкомпонентных записях.

В отношении первых вступлений по годографу определяется направление поляризации продольных волн. Направление поляризации волн *P–SV* оценивается на основе предположения, что отношение скоростей волн *P–SV* составляет 2:1. Изменение осей по отношению к направлениям поляризации, а также совместное применение *f–k* фильтрации в связи с кажущимися скоростями делают возможным расчленение полного волнового поля на нижеследующие четыре типа волн: нисходящие продольные, восходящие продольные, нисходящие *P–SV* и восходящие *P–SV*.

GEOPHYSICAL TRANSACTIONS 1987
Vol. 33. No. 1. pp. 41–55

OFFSET VERTICAL SEISMIC PROFILING FOR EXPLORING COMPLICATED AREAS

Helmut HOFFMANN and Volker KRUG*

Offset Vertical Seismic Profiling (OVSP) is applied routinely on an increasing scale to solve complicated exploration problems. In particular, the method is applied in hydrocarbon exploration under seismically unfavourable conditions such as near-surface complications, salt tectonics or restricted accessibility of the prospect area.

The method derived from zero-offset VSP allows structural investigations over distance of some kilometers around the well, and lithologic interpretation, too. For certain layer complexes the interpretation of the wave field data yields longitudinal and shear-wave velocities, anisotropy as well as attenuation information. Based on spatial distribution of the wave parameters and derived values, structural and lithological changes in the vicinity of the well are studied. Some aspects of field measurements, the processing sequence, and survey results are described.

Keywords: vertical seismic profiles, offset VSP, velocity, attenuation, raypath, P-wave, S-wave

1. Introduction

It is not a new idea to use well-seismic surveys for the geologic interpretation of the near-well area or to support and complement surface-seismic measurements. Mention is made here of the many years of fundamental research work done in the Soviet Union [GAL'PERIN 1971, 1982]. In recent years, it has become clear from SEG and EAEG meetings that interest in these surveys has strongly increased in western countries too. The tendency is evident to investigate the vicinity of deep wells by seismic surveys with energy excitation further from the well site (so-called offset vertical seismic profiling – OVSP). In the GDR, OVSP surveys have routinely been executed for 10 years, e.g. KÖHLER and KRUG [1975]; KRUG et al. [1978].

At present, OVSP surveys are mainly conducted for the solution of tasks in hydrocarbon exploration up to target depths of about 5000 m. Above all, OVSP is applied for the undershooting of inhomogeneities of the overburden, i.e. undershooting of Mesozoic fault zones, of waters or shore zones, of densely populated or inaccessible areas, etc. Finally, the OVSP has become a standard tool in areas with complicated salt tectonics. OVSP surveys have also been applied in the exploration of ore and for special tasks in the exploration of

* VEB Kombinat Geophysik Leipzig, Bautzner Strasse 67, GDR – 7024
Paper presented at the 31st International Geophysical Symposium, Gdansk, 30 September–3 October, 1986

potassium salts where signals up to 160 Hz could be recorded when the charge weight was reduced to 80 g. Furthermore, the application of OVSP is imaginable for the solution of tasks in coal exploration and in engineering geophysics, too.

2. Measurement principles and wave field

The planning of single measurements, especially of the shot points, is done by modelling according to geological and geometric aspects. In *Fig.1* the scheme of a measurement is presented. In the vicinity of the source a control probe is installed, if possible in the raypath of the direct wave. The recording of the direct wave enables accurate determination of statics and of wave attenuation. The waves travelling through the medium are recorded in the borehole by a highly

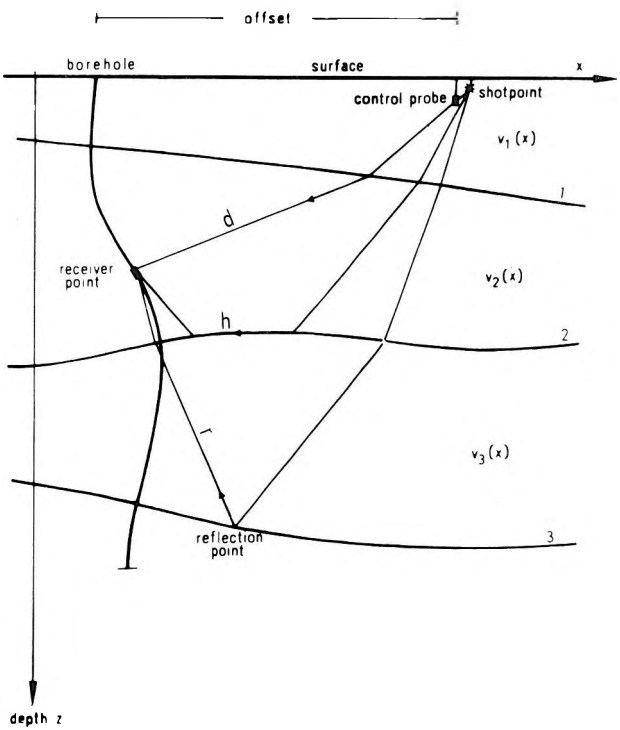

Fig. 1. Principles of offset vertical seismic profiling (OVSP)
1, 2, 3 — horizons; *d* — direct wave; *h* — head wave; *r* — reflected wave

1. ábra. A távoli gerjesztésű vertikális szeizmikus szelvényezés (TVSP) elve
1, 2, 3 — határfelületek; *d* — direkt hullám; *h* — fejhullám; *r* — reflektáló hullám

Рис. 1. Принцип вертикального сейсмического профилирования с выносом
1, 2, 3 — горизонты; *d* — прямая волна; *h* — головная волна; *r* — отраженная волна.

sensitive probe consisting of a group of vertical seismometers or a multicomponent system. The receiver intervals within the borehole vary between 10 and 60 m according to the requirements and the measurement geometry.

In Fig.1 different wave types important for interpretation are shown schematically. The direct wave can be observed as a *P*-wave (on the first arrival) or, especially with increasing offset, as a *PS*-wave or, more rarely, as a pure *S*-wave. Direct *PS*-waves are often very strong thereby disturbing the correlation of the upgoing reflected *P*-waves. Moreover, sometimes distinct converted waves occur travelling up to the reflector as *P*-waves and reflected as *S*-waves (*PS* reflections). Principally, all the multiples which can clearly be identified are suitable for interpretation too, but in the case of a complicated overburden their practical use is very restricted.

At relatively great offset, head waves may also appear—but these are weak and mostly highly distorted by interference with very strong supercritical reflections. These supercritical reflections of reflection angles of 40 to 65° are also useful for interpretation because they enable the investigated area to be delimited.

3. Processing sequence

A package of special programs is available for processing and interpreting OVSP surveys *(Fig.2)*. The recorded data are demultiplexed and sorted to produce the "raw time section" (right column of the flow chart). After that, statics are calculated and applied, whereby the position of the control probe is used as a reference point considering the raypath geometry roughly. In the next processing step the regular noise is eliminated by a multichannel filtering technique successively performed for regular noise cut-off. Finally, deconvolution is done taking into account the signal of the direct wave.

If desired cumulative attenuation can be determined using the signals of the direct wave at the control probe and the depth probe. By division of the spectra of both signals the attenuation k is determined from the slope of the frequency-dependent quotient of the spectra [e.g. RAIKES and WHITE 1984].

Knowledge on velocities is gained from the traveltimes of the first arrivals (left column of the flow chart). By the iterative solution of the direct and inverse kinematic problem improved velocities are calculated, taking an approximate model (velocities, geometry) as a basis. After each computation cycle the question has to be answered whether the new velocity distribution differs essentially from the input. In case of greater deviations from a threshold the computation needs to be re-started using the new velocities and so on. Usually a threshold of about 2% is taken. After successful improvement of the velocities the modelling of the reflected waves is done using the best velocities. The time-depth transformation of the time section (lower part of the flow chart) is executed by a special migration program or manually (in complicated cases).

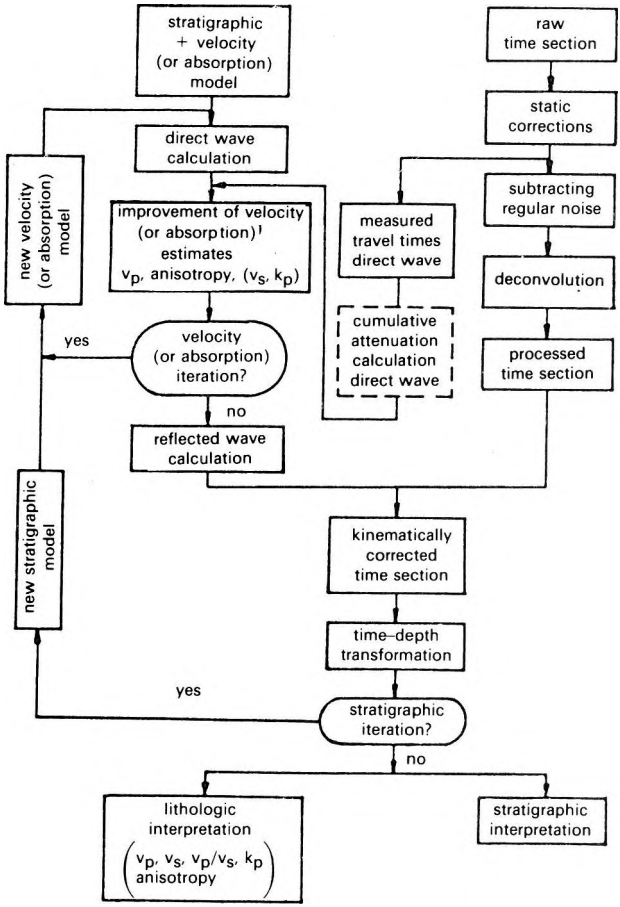

Fig. 2. Flow chart of OVSP processing

2. ábra. TVSP feldolgozás folyamatábrája

Рис. 2. Схема обработки данных в методе ВСП с выносом.

In comparison with the original stratigraphic (depth) model, its validity is tested. If there are striking structural changes, the whole processing sequence including the velocity determination has to be repeated iteratively. The cycle can be stopped if the stratigraphic input and output models (including the velocity-dependent values) are of sufficient coincidence. Now the processing can be finished and the geological interpretation may start.

4. Improvement of velocities and attenuation

The raypaths from the source to the receiver position within the borehole are more complicated when using offsets as shown by YOUNG et al. [1984]. We suppose [cf. KRUG et al. 1981] that the waves propagate through a layered medium with nearly unique layer velocities and with interfaces of different dips and curvatures. Furthermore, deviations of the borehole are considered. By solving the direct kinematic problem the raypaths are calculated assuming a plausible depth and velocity model. It should be noted that horizontal as well as vertical velocity gradients may occur within the sequences, and anisotropy too. From the solution of the direct problem raypaths and corresponding incidence angles are defined for each receiver point. If the supposed model is correct, the sum of the partial traveltimes would be equal to the measured traveltime. Hence, this fact leads for all the receiver points in the complex of m layers to the following equation system *(Fig.3)*:

$$\sum_{i=1}^{m} \frac{r_{ij}}{v_i(x_{ij}, A_i(\varphi_{ij}))} = t_{mj}$$

where

r_{ij} – raypath in layer i
x_{ij} – horizontal coordinate of raypath
v_i – interval velocity
$A_i(\varphi_{ij})$ – anisotropy in layer i, φ_{ij} – incident angle
t_{mj} – measured time in position j in layer m

As a rule, the difference Δt between the measured travel time t_{mj} and the calculated time t_{cj} is not equal to zero so that the above-mentioned equation system has to be solved by changing v_i (as the unknown variable). Possible changes of r_{ij} (or $A_i(\varphi_{ij})$) with regard to Δt are negligible in comparison with the influence of v_i for the mathematical solution of the inverse problem.

We overcome the problem by solving the inverse kinematic problem. Besides the Levenberg–Marquardt algorithm we tested the more empirical procedure of minimizing the traveltime difference Δt realizing a careful reduction of Δt iteratively in small steps taking into account the slope of the traveltime curve and the parts of traveltimes in the single layers [KRUG et al. 1981]. In our experience the error of the v_P layer velocities does not exceed 3%. The values v_i determined according to the equation system are attached to a mean coordinate $\bar{x}_i$ (position of the centre of gravity of all the raypaths in one layer) and a mean incident angle $\bar{\varphi}_i$ (mean value of the incident angles of all the raypaths in one layer), and we write $v_i(\bar{x}_i, A_i(\bar{\varphi}_i))$. In this way several values of v_i can be obtained from one VSP if the receiver points are situated in several layers and the number of layers is less than the number of receiver points in the layers. Taking Fig.3 as our example, it means that if receiver points are located in all

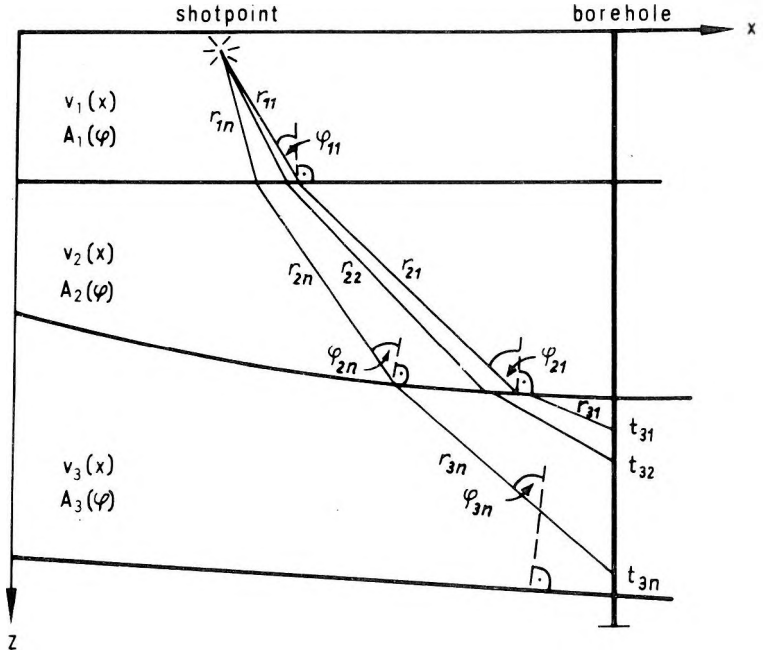

Fig. 3. Raypath scheme for direct waves
r_{ij} — raypath in layer i; $v_i(x)$ — interval velocity; $A_i(\varphi)$ — anisotropy in layer i; φ_{ij} — angle of incidence; t_{ij} — measured time in position j in layer i

3. ábra. A direkt hullám sugárútvázlata
r_{ij} — sugárút az i-ik rétegben; $v_i(x)$ — intervallum sebesség; $A_i(\varphi)$ – anizotrópia az i-ik rétegben; φ_{ij} — beesési szög; t_{ij} — mért beérkezési idő az i-ik réteg j-ik geofon-helyén

Рис. 3. Схема лучевого пути прямой волны:
r_{ij} — лучевой путь в i-том слое; $v_i(x)$ — интервальная скорость; $A_i(\varphi)$ — анизотропия в i-том слое; φ_{ij} — угол вхождения; t_{ij} — измеренное время прихода в пункте j-того сейсмоприемника i-того слоя.

three layers and the equations for the receivers in each of them can be set up, three values of v (with different $\bar{x}$ and $\bar{\varphi}$) can be obtained in the first layer, two values of v in the second layer, and one in the third layer. Furthermore, most of the results come from several measurements of different offsets, but from the same profile direction. All the values $v_i(x_{ij}, A_i(\varphi_{ij}))$ are influenced both by the position (x) of the actual segments of the raypaths and by the anisotropy $A_i(\varphi_{ij})$. Therefore, the effects of the horizontal gradient (position x) and of anisotropy ($A_i(\varphi_{ij})$) must be separated from one another for each layer. This is done by solving the invers problem for the unknowns (horizontal gradient and anisotropy) again, where the horizontal gradient is approached as a function of first order. Deviations from linearity over the distance x are interpreted as indications for local anomalies within the sequence. In *Fig.4* anisotropy distributions

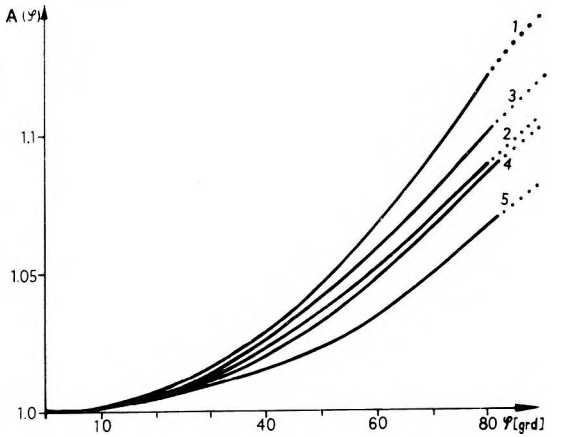

Fig. 4. Anisotropy of longitudinal waves in geological complexes
1 — Pleistocene – Upper Cretaceous; 2 — Lower Cretaceous – Keuper; 3 — Muschelkalk; 4 — Lower Triassic; 5 — Zechstein

4. ábra. Longitudinális hullám anizotrópiája a különböző összletekben
1 — pleisztocén – felsőkréta; 2 — alsókréta – felsőtriász; 3 — középső triász; 4 — alsó triász; 5 — felső perm

Рис. 4. Анизотропия продольных волн в различных толщах:
1 — плейстоцена до верхнего мела; 2 — нижнего мела до верхнего триаса; 3 — среднего триаса; 4 — нижнего триаса; 5 — верхней перми.

$A(\varphi)$ for single geological sequences are compiled which were gained from measurements in the North German Basin [KRUG and SCHEIDT 1985]. Obviously, the values decrease with increasing depth and age, respectively.

The velocity improvement of the shear-wave can be accomplished in the same way. For that purpose special measurements are normally not necessary. As is known, direct converted *PS* waves near the surface are more clearly recognizable when larger offsets are used and strong velocity contrasts exist. Their *S*-wave component can be used to determine v_S. Hence, the v_P/v_S ratio is defined.

The layer attenuation coefficients k_P are derived in a similar way from the cumulative attenuation of the direct wave. But the occurring error of 30 to 50% is much higher due to the uncertainties in the determination of spectra quotients.

5. Time–depth conversion

As shown in the flow chart of Fig. 2, iterative improvement of velocities and anisotropies is mandatory for the time–depth conversion. The conversion itself is rather difficult. An impression of the problems is given by DILLON and THOMSON [1984], who dealt with simplified conditions of horizontal layering and a vertical velocity function. In practice such assumptions are not fulfilled at least for surveys of offsets greater than 1 km therefore, we followed the way described

formerly [KRUG et al. 1978]. By solving the direct kinematic problem (taking the known model of the overburden, as well as velocity and anisotropy distribution as a basis), the reflected wave coming from a definite horizon (horizontal, dipping or curved) is calculated for all the receiver points along the well. First, the position of the horizon is supposed to be known and is then shifted parallely into different depths. To each reflection point R_{kl}, three values (coordinates x_{kl}, z_{kl}, and the (theoretic) traveltime t_{kl} are assigned, where k is the serial number of trace on the time section, l is the number of the depth variation. These data allow one to construct a template map in the (t, z) plane.

For better visualization and interpretation, time sections and template maps are corrected kinematically. This is done so that the traveltimes of the main target horizon calculated theoretically are shifted to form a uniform traveltime. When the main target horizon is dipping or curved the depth lines on the template map over the time section reflect dips or curvatures. For the measured traveltimes the corresponding depths are determined on the template map, but the horizontal coordinate x_{kl} of the reflection point has to be considered. The whole procedure must be repeated if there is no agreement with the basic model. At present, because of the complexity of the models the work is still done manually in parts. Automatic time–depth conversion to CDP time sections is in preparation.

By several surveys of different offsets in one direction a certain multiple coverage can be achieved. As a rule, we are satisfied with one subcritical survey per azimuth to secure a good tie of the horizons in the immediate neighbourhood of the well, and the improvement of the velocities. Beyond this, 1–2 surveys in the supercritical range are executed. Accuracies of 10 to 50 meters in the vertical and horizontal directions are attainable depending on the complexity of the geological setting.

6. Examples

Figure 5 shows the variation of petrophysical parameters in the vicinity of a borehole derived from four measurements with different offsets in one direction. The parameters refer to a layer of 200 m thickness in a depth of 2600 m which is interesting for oil prospecting. Velocities and attenuation values run contrarily. The v_P/v_S ratio decreases. With regard to lithological interpretation in this area no essential variations of the petrographic composition were expected. Consequently, the increased attenuation and the decreased velocities indicated an increase of porosity and a change of the pore filling, respectively.

Later the well drilled in this area came into production proving a higher inflow of hydrocarbons, especially an increase of the gas content. Quantitative interpretation failed because of the relatively great errors of the values. Special investigations in the laboratories, for instance calibrations of core samples, should be executed.

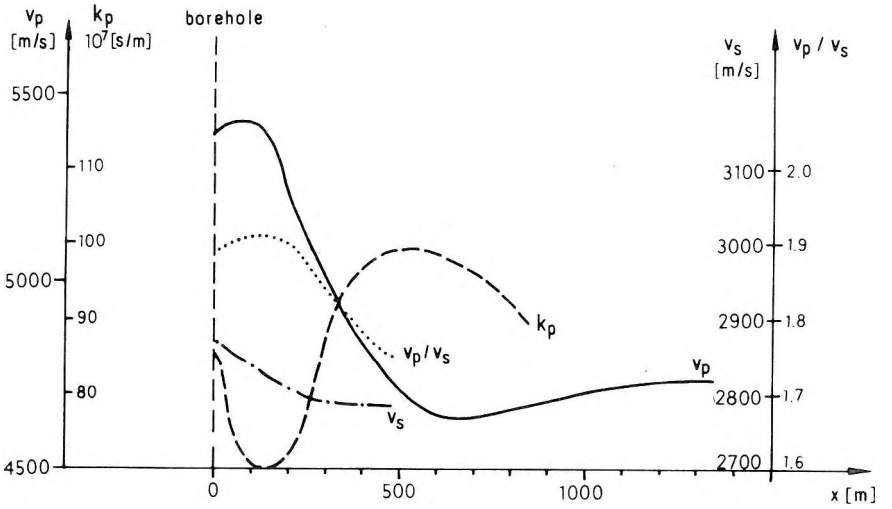

Fig. 5. Variation of petrophysical parameters in the vicinity of a borehole [after KRUG et al. 1981]
v_P — velocity of longitudinal wave; v_S — velocity of transverse wave; k_P — coefficient of absorption for *P*-waves

5. ábra. Kőzetfizikai paraméterek változása egy mélyfúrás környezetében [KRUG et al. 1981 után]
v_P — *P*-hullám sebessége; v_S — *S*-hullám sebessége; k_P — *P*-hullám abszorpciós koefficiense

Рис. 5. Изменение петрофизических параметров в окрестностях буровой скважины [по KRUG et al. 1981]:
v_P — скорость продольных волн; v_S — скорость поперечных волн; k_P — коэффициент абсорбции продольных волн.

Commonly, the tracing of horizons below salt bodies by means of surface seismics is impossible. In such areas OVSP surveys help considerably to reduce or even to abolish "white spots". An OVSP "raw" time section of a supercritical undershooting of the flank of a salt dome is shown in *Fig. 6*. A few wave types are recognizable, viz. the direct *P*-wave, the direct *S*-wave, supercritical reflected waves, and the downgoing *PS*-waves. *Figure 7* shows the same time section after multichannel filtering: the upgoing waves appear clearly. The time section is corrected kinematically (according to values gained from the solution of the direct kinematic problem for reflected waves) so that the main target horizons H_1 and H_2 run at a nearly uniform traveltime. The quality and the continuity of the reflectors are good over almost 2000 m. Furthermore, a reflection appears within the salt (H_0).

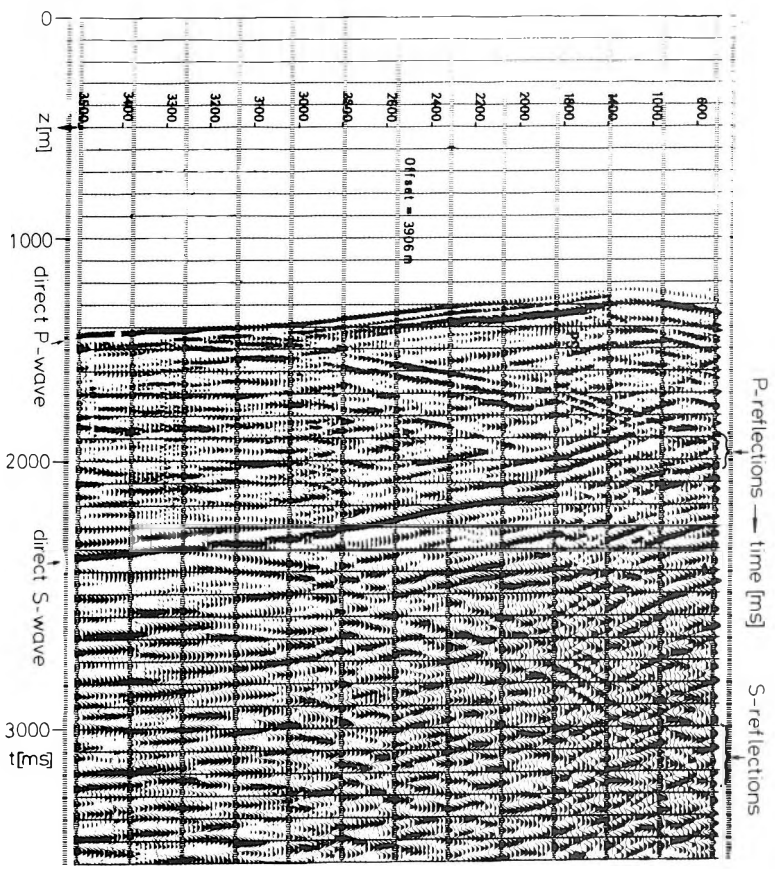

Fig. 6. Unprocessed OVSP time section of a supercritical undershooting of a salt dome flank

6. ábra. Feldolgozás előtti TVSP időszelvény, sódóm alól kapott, kritikusnál nagyobb szögű reflexiókkal

Рис. 6. Временной разрез ВСП с выносом до обработки с отражениями под углами выше критических, полученными из-под соляного купола.

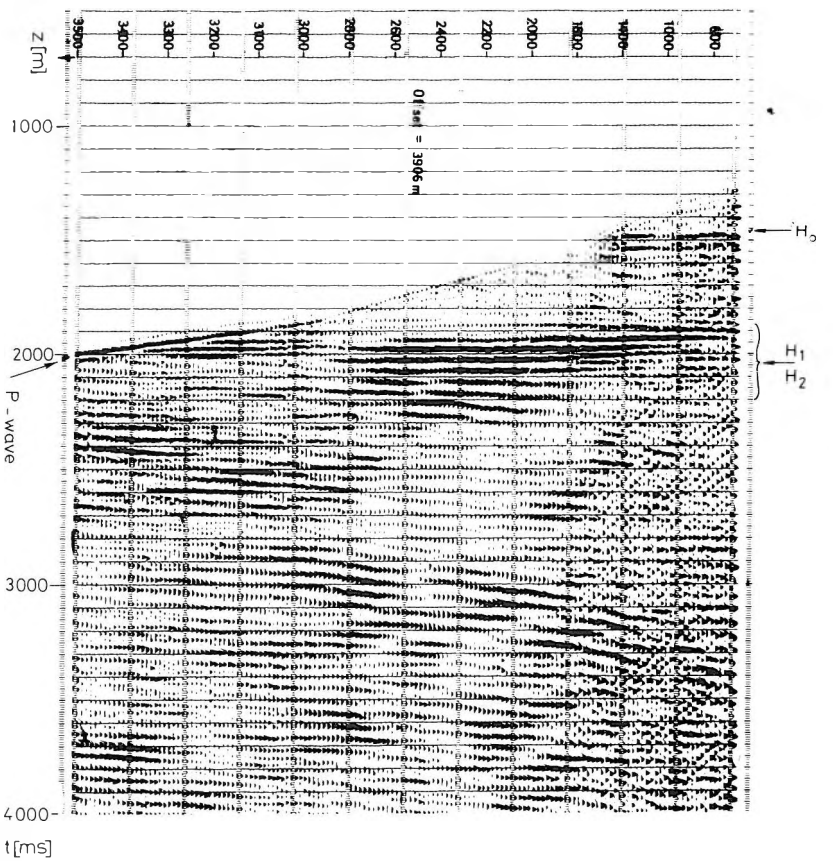

Fig. 7. Processed and kinematically corrected time section of Fig. 6

7. ábra. A 6. ábra időszelvényének feldolgozott és kinematikailag korrigált változata

Рис. 7. Временной разрез рис. 6 после обработки и кинематической поправки.

In *Fig. 8* a surface–seismic time section crossing a salt dome can be seen. The target horizons between 1.6 to 2.0 s is not traceable despite optimum processing. But, by means of an OVSP survey, the gap in the reflection seismic result can be filled. Two OVSP time sections are inserted into the surface–seismic section given in *Fig. 9*. The reflections on the surface–seismic section can be followed over the OVSP sections. In *Fig. 10* the depth results are presented: the surface–seismic results are indicated by dotted lines, the horizons from OVSP are given by continuous or broken lines. The efficiency of the combination of reflection seismic and OVSP measurements is evident from Fig. 10.

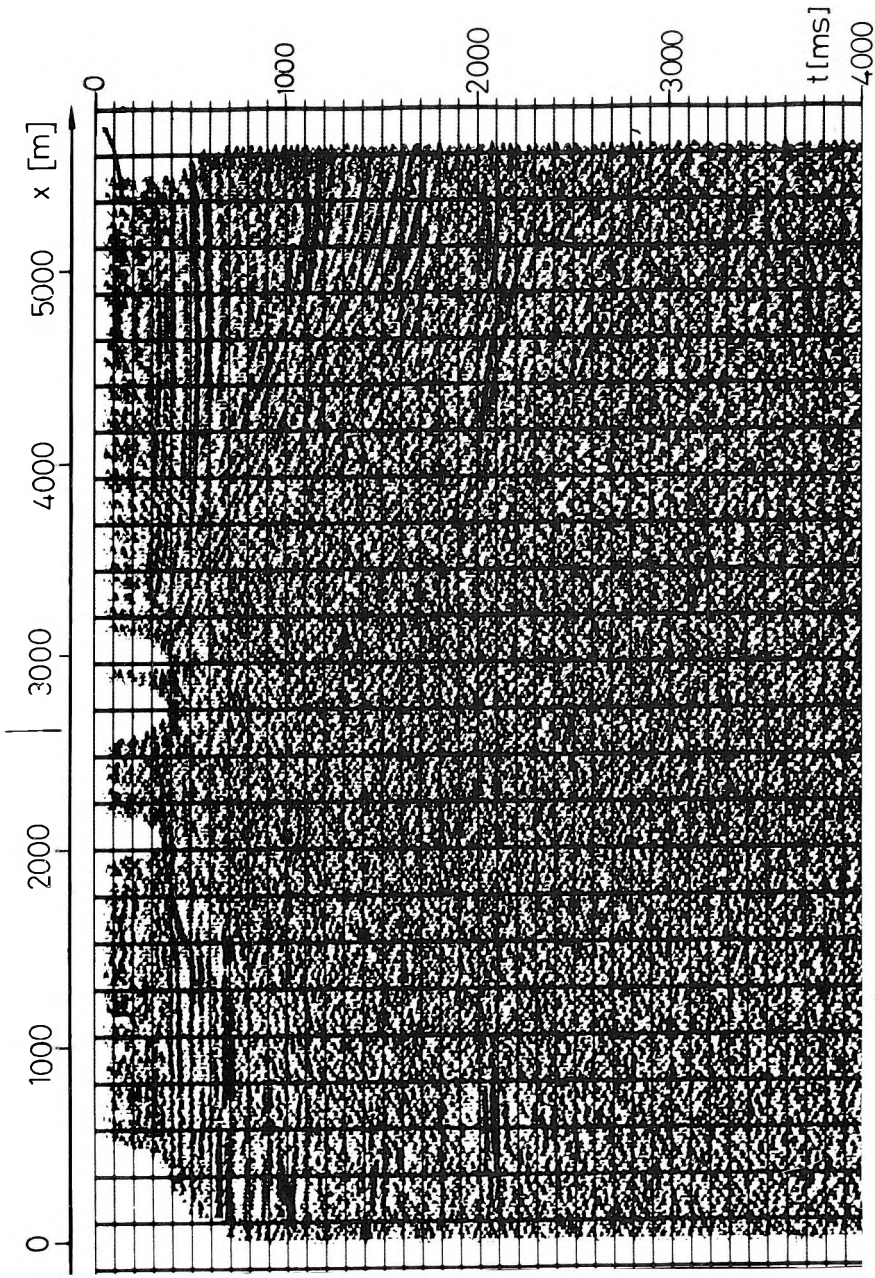

Fig. 8. Surface-seismic time section crossing a salt dome

8. ábra. Sódómot harántoló felszíni szeizmikus mérés időszelvénye

Рис. 8. Временной разрез сейсмического профиля, измеренного с дневной поверхности через соляной купол.

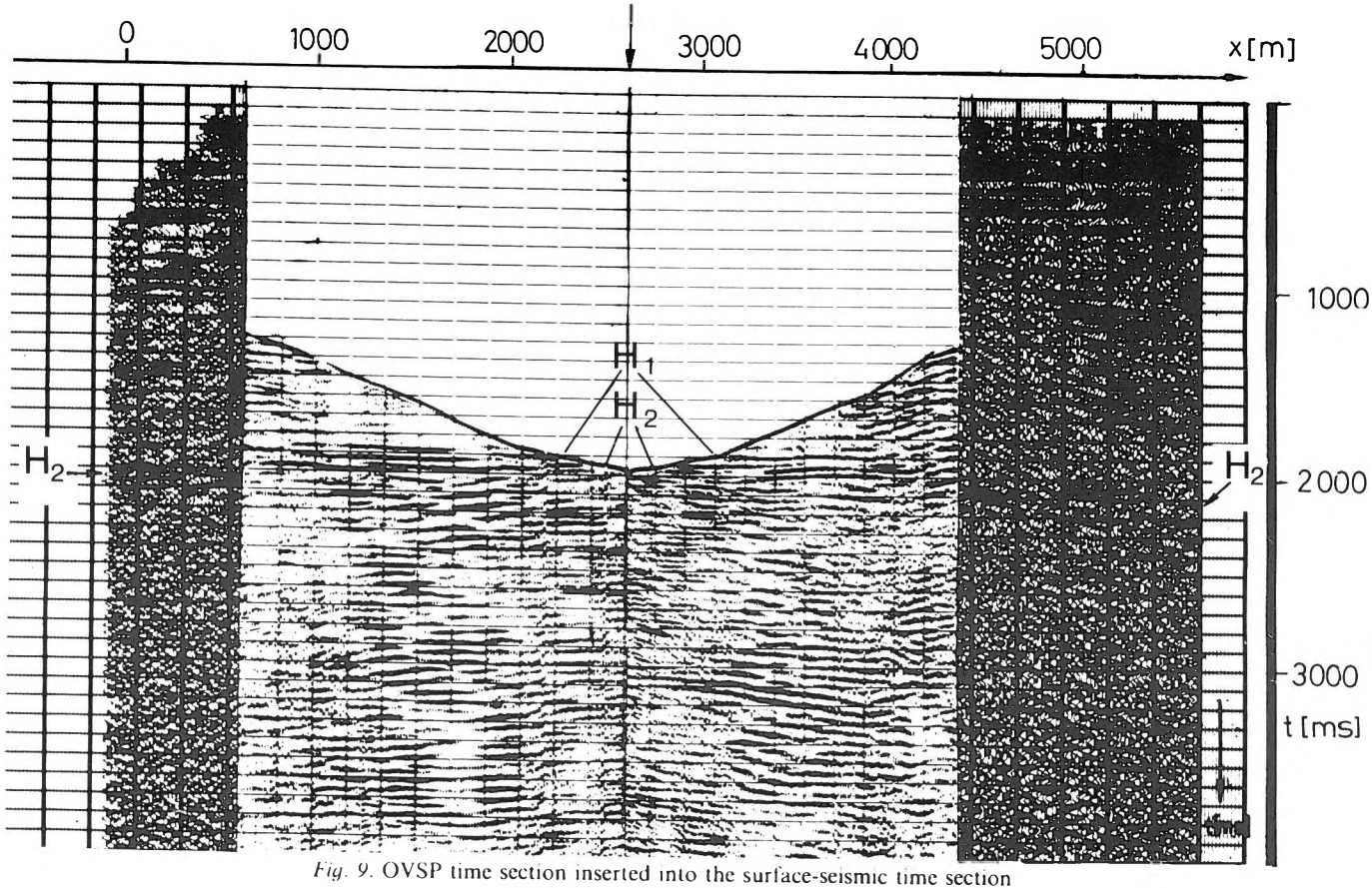

Fig. 9. OVSP time section inserted into the surface-seismic time section

9. ábra. TVSP időszelvény beillesztve a felszíni szeizmikus mérés időszelvényébe

Рис. 9. Временной разрез ВСП с выносом, включенный во временной разрез по измерениям с дневной поверхности.

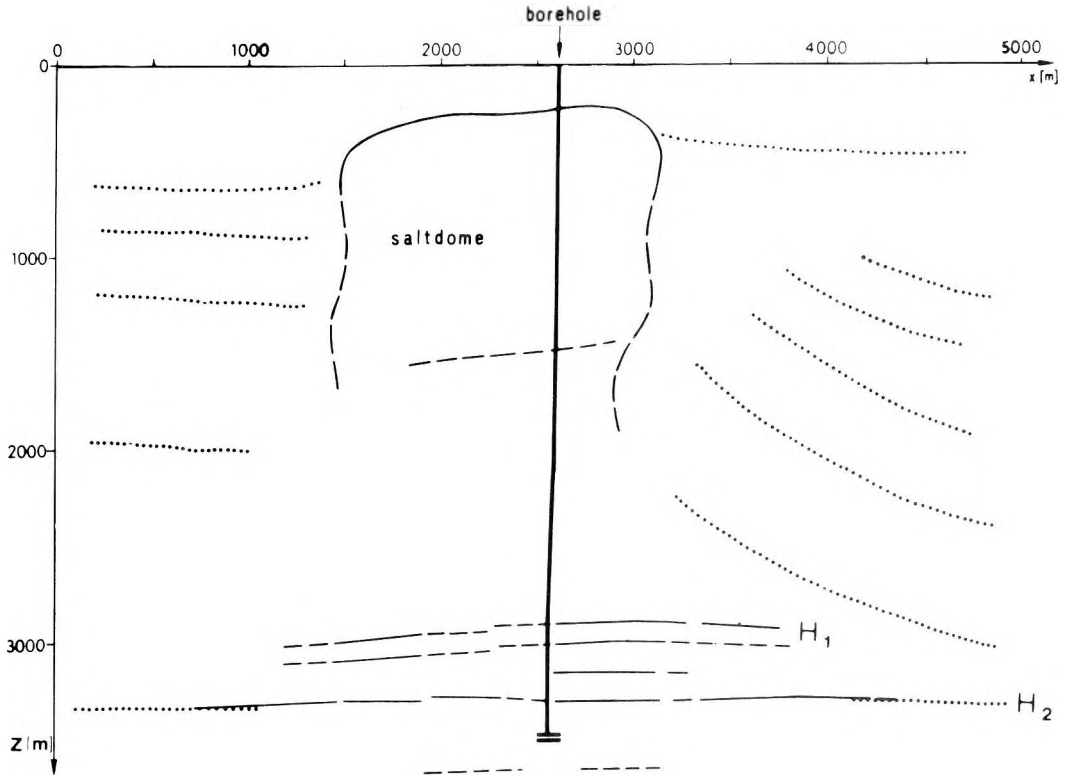

Fig. 10. Depth section converted from time section of Fig. 9. Dotted lines mark results of surface-seismics, continuous and broken lines those of OVSP

10. ábra. A 9. ábra időszelvényének mélységszelvénye. A pontozott vonalak a felszini mérés eredményét, a folyamatos és szaggatott vonalak a TVSP eredményét jelölik

Рис. 10. Глубинный разрез по временному разрезу рис. 9. Пунктиром обозначены результаты измерений с дневной поверхности, а сплошными и прерывистыми линиями — результаты ВСП с выносом.

REFERENCES

DILLON P. B., THOMSON R. C. 1984: Offset source VSP surveys and their image reconstruction. Geophys. Prosp. **32,** 5, pp. 790–811

GAL'PERIN E. I. 1971: Vertical seismic profiling (in Russian). Nedra, Moscow, 264 p, English translation, SEG special publication No. 12, 1973, Tulsa

GAL'PERIN E. I. 1982: Vertical seismic profiling (in Russian). Nedra, Moscow

KÖHLER E., KRUG V. 1975: Reflexionsseismische Verfahren zur Erkundung subsalinarer Horizonte unterhalb tektonisch kompliziert gebautem Deckgebirges. Zeitschr. geol. Wissensch., Berlin **3,** 4, pp. 441–459

KRUG V., BAUM G., LANGE G. 1978: Special well shooting investigations in the surrounding of boreholes. Proc. 23rd Geophys. Symp. Varna, Sofia, pp. 223–235

KRUG V., BAUM G., WINDGASSEN W. 1981: Nutzung bohrlochseismischer Spezialmessungen zur Untersuchung petrophysikalischer Parameter in der Umgebung von Tiefbohrungen. Zeitschr. geol. Wissensch. Berlin **9,** 8, pp. 851–862

KRUG V., SCHEIDT W. 1985: Zur Anisotropie petrophysikalischer Kenngrössen in seismischen Schichtkomplexen. Zeitschr. geol. Wissensch. Berlin **13,** 4, pp. 483–497

RAIKES S. A., WHITE R. E. 1984: Measurement of earth attenuation from downhole and surface recordings. Geophys. Prosp., **32,** 5, pp. 892–919

YOUNG C. B., MONASH C. B., TURPENING R. M. 1984: Computer modeling of vertical seismic profiling. Geophys. Prosp., **32,** 5, pp. 851–870

TÁVOLI GERJESZTÉSŰ VSP BONYOLULT TERÜLETEK KUTATÁSÁRA

Helmut HOFFMANN és Volker KRUG

A távoli gerjesztésű vertikális szeizmikus szelvényezést (TVSP) egyre inkább rutinszerűen alkalmazzák bonyolult kutatási feladatok megoldására. A módszer különösen a szénhidrogén-kutatás szeizmikus szempontból kedvezőtlen feladatainál alkalmazható, például felszínhez közeli bonyolult szerkezet, só-tektonika, vagy a kutatandó terület korlátozott megközelíthetősége esetén.

A lyukszáji gerjesztésű VSP-ből levezetett módszer teszi lehetővé a fúrólyuk körüli néhány kilométeres terület szerkezeti és kőzettani értelmezését. Bizonyos rétegsorokra a hullámtér kiértékelése longitudinális és nyíróhullám sebesség adatokat, továbbá anizotrópia és csillapodási információt szolgáltat. A hullámparaméterek és a származtatott értékek térbeli eloszlására alapozva a fúrólyuk közelében tanulmányozhatjuk a szerkezeti és kőzettani változásokat.

ВЕРТИКАЛЬНОЕ СЕЙСМИЧЕСКОЕ ПРОФИЛИРОВАНИЕ С ДАЛЬНИМ ВОЗБУЖДЕНИЕМ В ИЗУЧЕНИИ ПЛОЩАДЕЙ СО СЛОЖНЫМ ГЕОЛОГИЧЕСКИМ СТРОЕНИЕМ

Гельмут ГОФМАН и Фолькер КРУГ

Вертикальное сейсмическое профилирование с выносом все чаще применяется в серийном порядке для решения сложных задач, возникающих при геологоразведочных работах, особенно задач поисков и разведки нефти и газа, неблагоприятных для применения сейсмических методов, как, например, в случае сложных структур близ поверхности, в случае проявления соляной тектоники или в случае низкой проходимости изучаемого района.

Способ, представляющий дальнейшее развитие вертикального сейсмического профилирования с устьевым возбуждением, обеспечивает возможность структурной и литологической интерпретации всего участка размером в несколько кв. км, прилегающего к скважине. В случае определенных типов геологического разреза интерпретацией волнового поля обеспечиваются данные по скоростям продольных и скалывающих волн, а также по анизотропии и затуханию. На основе пространственного распределения волновых параметров и разчетных значений создается возможность изучения структурных и литологических изменений в окрестностях скважины.

GEOPHYSICAL TRANSACTIONS 1987
Vol. 33. No. 1. pp. 57–65

EFFICIENCY OF GEOPHONE PATTERNS IN 3D-SEISMICS

Bernd THOMAS and Rolf PILLING*

Due to the increasing use of areal spreads in reflection seismic prospecting the directivity properties of geophone patterns must be studied again besides other problems. Contrary to 2-D profiling, an azimuth-dependent directivity analysis is necessary. Three different patterns are presented and discussed with regard to their directivity and practical realization.

Keywords: 3-D seismics, geophone pattern, noise, signal-to-noise ratio, directivity, attenuation

1. Introduction

In recent years the application of areal reflection seismic surveys has seen a world-wide increase on a big scale on land as well as offshore. For the VEB Kombinat Geophysik Leipzig these measurements have become more and more essential. In this connection the choice of the 3-D measuring parameters to obtain a sufficiently high S/N-ratio is of particularly great importance for several reasons. Due to the high expense necessary for 3-D measurements the optimization or minimization of the measuring parameters is a must. The primary S/N-ratio of the received waves is highly influenced by the shot and geophone patterns as well as by the parameters of the geophones and of the recording filters. The effects of the recording filters and of the geophone responses are not considered in the following since there are no essential differences against 2-D surveys. In shot seismics, patterns must be rejected for economic reasons. Before 3-D surveys are started it is necessary to obtain a complete overview on all parameters of the survey area. A detailed seismo-geological model must be designed which comprises the minimum and maximum depths of all horizons to be explored, the intervals of the mean velocities, and the dips. All the methodological and technological viewpoints necessary or possible parameters of the layout, existing knowledge on signal parameters as mean values and standard deviations of primaries and regular noise, the predominating frequency, wavelengths or apparent velocities must be collected and taken into account in survey projecting [HEINITZ 1959, PUZYREV 1957, LOZOVSKAYA 1961].

The tasks of geophone patterns are the following:

— Wavelength filtering, i.e. suppression of regular noise, as surface waves;

* VEB Geophysik Leipzig, Bautzner Str. 67, Leipzig GDR-7024
Paper presented at the 31st International Geophysical Symposium, Gdansk, 30 September–3 October, 1986

— Stochastic suppression of random noise;
— Distortion-free and quasi-synchronous superposition of useful signals.

Considering geophone patterns for 2-D and 3-D surveys, the main difference is that in 3-D measurements the azimuths of regular noise caused by wave generation varies from 90°–270° or 270°–90° respectively depending on the direction of observation. The assumption made in 2-D surveys that noise propagates along the seismic line is not valid in 3-D surveys *(Fig. 1)*. Due to the areal distribution of generation and reception points the azimuth of the noise arriving at the pattern practically changes at each generation, thus covering the above mentioned interval *(Fig. 2)*. For 2-D measurements only the azimuth in the direction of the line is important when the directivity is to be determined.

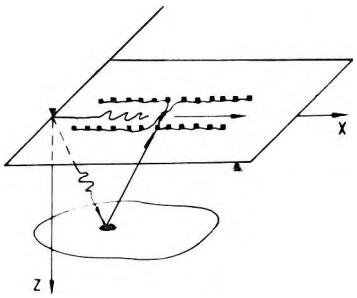

Fig. 1. Wave propagation in 2-D profiling

1. ábra. Hullámterjedés 2-D szelvényezés esetén

Рис. 1. Распространение волн при двухмерном профилировании

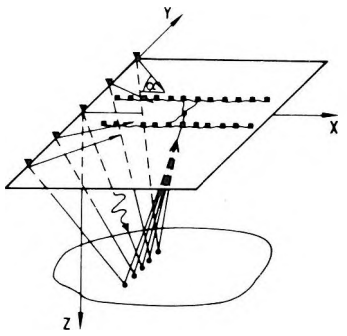

Fig. 2. Wave propagation in a 3-D survey

2. ábra. Hullámterjedés 3-D mérés esetén

Рис. 2. Распространение волн при трехмерном профилировании

2. Design of geophone patterns

For the design of efficient patterns for 3-D surveys it is necessary to involve systems which provide an omnidirectional and possibly constant attenuation of surface waves. The minimization of the technological efforts is essential in this connection. When deciding on a geophone pattern, one must:

a) determine the maximum possible basis of interference for the target or key horizons as a function of the expected signal frequencies or the required resolving power, taking into account the high-cut filtering of the pattern (curvature of the traveltime curve, traveltime differences due to surface effects considering the muting curve);

b) keep the condition

$$D_B \leq GGA \qquad \begin{array}{l} D_B \text{ — pattern length} \\ GGA \text{ — geophone group interval} \end{array}$$

in order to prevent signal mixing at the depth points and for technological reasons;

c) predict the influence of the intensity of regular and random noise in relation to reflection energy considering the 3-D layout which is to be used.

The implication of the parameters and data mentioned under point a) can be considered as given, if the known formulae for homogeneous field patterns, i.e. systems with identical sensitivities of the elements and uniform spacing between elements, are used. The response of an areal geophone array as it is required for 3-D surveys is inhomogeneous and varies as a function of the azimuth of the noise arriving at the array. In order to determine cutoff values for signal distortion it seems expedient to estimate these data on the basis of the prevailing directivity which is valid in the specific azimuth. For that reason the known formula is applied:

$$\lambda^* = \frac{v^*}{f} \tag{1}$$

Inserting the cutoff parameters of the useful waves into equation (1), we get

$$\lambda^*_{min} = \frac{v^*_{min}}{f_{max}} = v^*_{min} t_{min} \tag{2}$$

where

λ^*_{min} — minimum apparent wavelength of the reflection from the shallowest target horizon at maximum reception distance

v^*_{min} — minimum apparent velocity of the reflection from the shallowest target horizon at maximum reception distance and muting

f_{max} — upper cutoff frequency of the signal

t_{min} — $1/f_{max}$

The cutoff value, λ^* (cutoff for useful waves) may be taken from each actual amplitude response out of the attenuation range between 0 and -3 dB, depending on the permitted maximum degree of signal distortion. The following condition must be satisfied:

$$\lambda^*_{min\,(geol.\,model)} \geq \lambda^*_{limit} \text{ (from array response)} \tag{3}$$

The value of λ^*_{min} can be derived from the minimum apparent velocity of the seismogeological model, and is based on the following relationships:
From the travel-time curve

$$t = \frac{1}{\bar{v}} \sqrt{4h_{min}^2 + x^2 \pm 4h_{min} x \sin \varphi_x} \tag{4}$$

where
h_{min} — vertical depth to the shallowest reflecting horizon
x — registration distance in the direction of the profile
φ_x — apparent dip angle of strata in the direction of the profile
$\bar{v}$ — mean velocity to h_{min}
follows the apparent velocity

$$v^*_{min} = \bar{v} \frac{\sqrt{4h_{min}^2 + x_{max}^2 + 4h_{min} x_{max} \sin \varphi_x}}{x_{max} + 2h_{min} \sin \varphi_x} \tag{5}$$

The λ^*_{min} (geol. model) value represents the minimum apparent wavelength of the signal for the minimum exploration depth h_{min} at the maximum possible offset x_{max} considering muting and dip angle φ_x. By satisfying conditional equation (3) it is ensured that waves of λ^*_{min} apparent wavelength do not fall in the attenuation domain of the directivity characteristics starting at λ^*_{limit}.

The mean λ^*_{limit} wavelength of geophone pattern variant A of Fig. 4 applied to 3-D measurement in the GDR is 83 m. The parameters h_{min}, $\bar{v}$, φ_x, x_{max} derived from the geological model have the values:

h_{min} = 640 m
$\bar{v}$ = 2140 m/s
φ_x = 10°
x_{max} = 600 m

From Eq. (5) it follows that the minimal apparent velocity $v^*_{min} \approx 3900$ m/s. The minimal apparent wavelength for $f_{max} = 40$ Hz is about 98 m, and satisfies Eq. (3).

The statistical effect of a geophone pattern is then maximum (theoretical maximum value is $\sqrt{n}$, n — number of geophones) when the geophones of one pattern have the same sensitivity, and the interval between the geophones of the pattern is greater than the radius of the ambient noise.

The first condition can practically be satisfied, the second one only incompletely. Commonly, this radius amounts to several decameters, hence, a maximum effect cannot be achieved due to the comparably small element spacing which is determined by signal distortion and required directivity. For that reason extended linear geophone arrays may be more advantageous than areal arrays of less extent if we consider the statistical effect.

The geophysicist has the task of finding suitable pattern parameters on the basis of known data of regular noise (surface waves, sometimes sound waves

too) as shown in *Table I.* He must observe the cutoff values which ensure, under the given conditions, the maximum attenuation. One must strive for an attenuation of the main noise components of ≥ 12 dB and of about 3... < 12 dB for the minor components, where those wavelengths approaching the cutoff wavelength of useful waves, i.e. near the band-pass of the response, are practically not attenuated (e.g. distorting refractions).

For 3-D surveys the number of geophones in a pattern, the pattern area and the technological effort have to be minimized, while ensuring as far as possible the mentioned azimuth-dependent attenuations.

Parameters	Surface waves	Sound waves
v[m/s]	200...400	318...348
f[Hz]	8...20	12...110
λ[m]	10...50 peak 25...30	3...29

Table I. Table of noise parameters

I. táblázat. Zajparaméterek táblázata

Табл. I. Таблица параметров волн помех

3. Results

In studying this problem we developed the analysis program VARIPAT which allows the calculation of responses of arbitrarily dimensioned field patterns. From the great number of already analysed geophone patterns—also in combination with source patterns—with regard to their attenuation capability against surface waves, the following three selected variants including one known from the literature (Prakla–Seismos 1982) are presented.

In *Fig. 3* their areal configurations are shown; *Table II* comprises the main data of these variants. From the areal extension of the variants it is seen that types (A) and (B) are suitable for array intervals of about 40–50 m and (C) for about 70–80 m. It must be stated that for an actual case only those patterns will be applied which do not involve for any occurring azimuth an extreme weighting of elements, thus preventing unwanted phase shifts of the signals and a limitation of directivity.

As a criterion for the efficiency of each of the three presented variants we suggest their attenuation capability within the range of the prevailing noise wavelengths $\lambda = 20...40$ m. Special investigations on the stochastic effect were not undertaken due to similar phenomena in 2-D surveys.

In order to compare the specific differences between the three variants, *Fig. 4* demonstrates the azimuth-dependent amplitude responses (at a position accuracy of the geophones of ≤ 0.2 m) for the azimuths 0°...90° in 15°-steps,

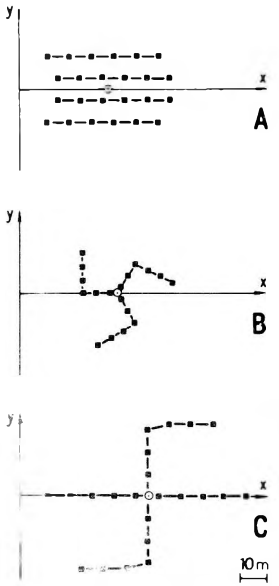

Fig. 3. Selected geophone patterns

3. ábra. Kiválasztott geofon csoportosítások

Рис. 3. Выбранные конфигурации группирования сейсмоприемников

Parameters / Variant	Number of geophons	Length [m] in direction x	Length [m] in direction y	Area [m²]
A	24	44	24	rectangular 1056
B	18	32	33	circular 1198
C	22	72	52	rectangular 3744

Table II. Table of parameters of selected geophone patterns

II. táblázat. A kiválasztott geofoncsoportok paramétereinek táblázata

Табл. II. Таблица параметров выбранных конфигураций группирования сейсмиприемников

Fig. 4. Directivity graphs of analysed geophone patterns
1 — variant (A); 2 — variant (B); 3 — variant (C)

4. ábra. A vizsgált geofoncsoportok iránykarakterisztikái
1 — (A) változat; 2 — (B) változat; 3 — (C) változat

Рис. 4. Характеристики направленности анализированных конфигураций группирования сейсмоприемников
1 — вариант (A); 2 — вариант (B); 3 — вариант (C)

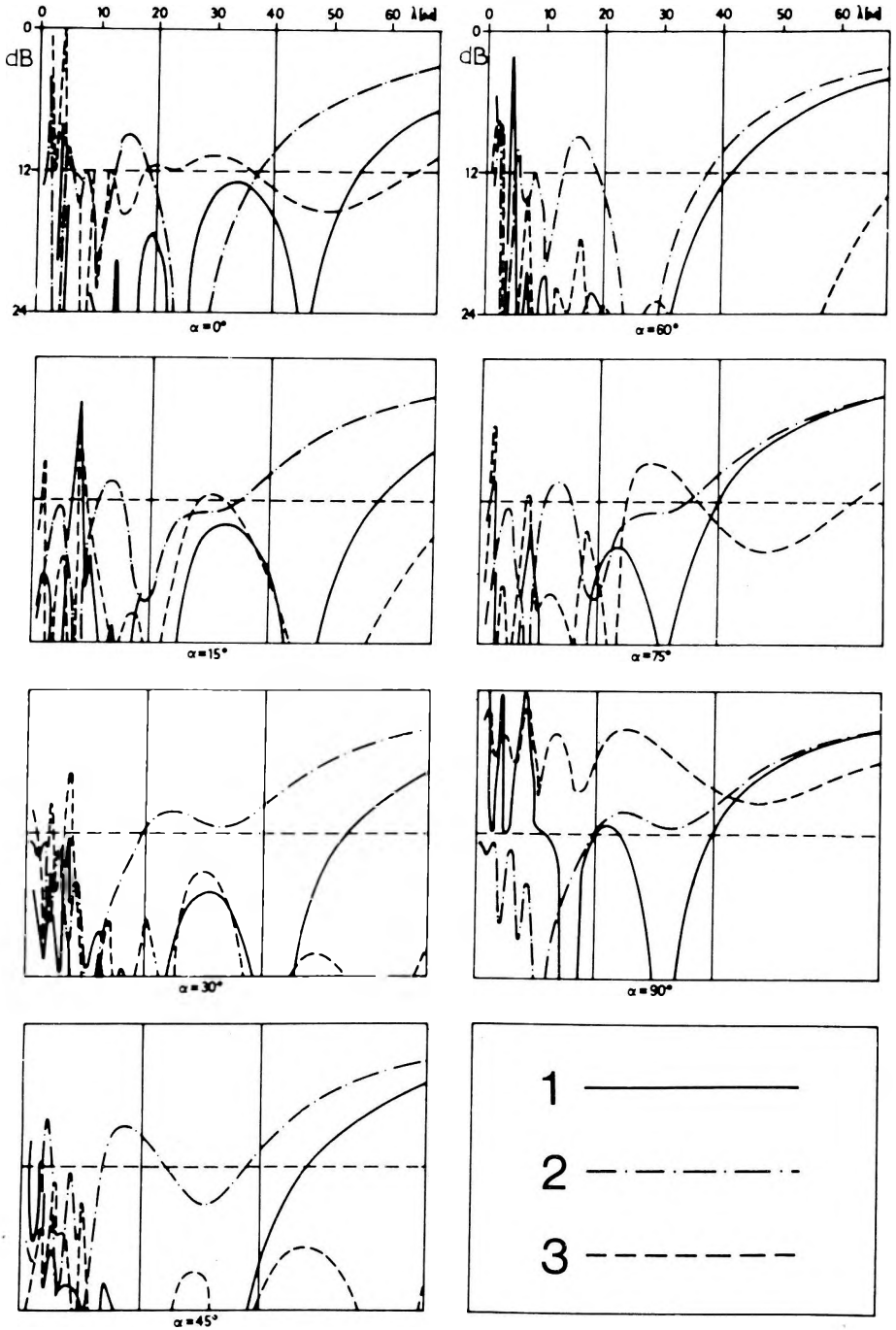
0 10 20 30 40 50 60 λ/d
dB
0
12
24
α = 0°
α = 60°
α = 15°
α = 75°
α = 30°
α = 90°
α = 45°
1
2
3

where the interesting wavelength range 20...40 m is presented in windows within the attenuation interval 0...24 dB. For practical purposes a minimum attenuation of 6...12 dB is required. In Fig. 4 the 12 dB limit is drawn with a dashed line.

Comparing the variants (A) and (B) in Fig. 4 which are designed for similar array intervals, it is easily seen that variant (A) provides constant attenuations of little more than 12 dB with one exception at $\alpha = 90°$. In the considered λ-interval, in no case does variant (B) ensure a complete 12 dB-attenuation. Thus, the advantage of variant (A) over (B) is obvious from the viewpoints of directivity and field technology, since less area (88%) is required, with simpler layout.

Considering, finally, variant (C), we can see that for most of the azimuths the 12 dB-limit cannot be kept constantly. This variant provides sufficiently high attenuation only for certain azimuths or azimuth ranges of $\alpha = 15°...60°$. Therefore, such patterns are only to be applied when exclusively using certain azimuth intervals. In 3-D surveys the α-range is fixed by the actual x- and y-offsets between source and reception points, and must be individually discussed for each system.

REFERENCES

Heinitz K. 1959: Das Problem der Bundelung von Geophonen. Freiberger Forschungshefte, **C66**, pp. 5–47, Akademie-Verlag, Berlin

Puzyrev N. N. 1957: On phase distortions and amplitude characteristics of long-base geophone arrays (in Russian). Prikladnaya Geofizika, **17**, pp. 3–15

Lozovskaya I. F. 1961: On areal geophone arrays (in Russian). Prikladnaya Geofizika, **31**, pp. 85–100

O. V.: Prakla-Seismos 1982: Information No. 35, 3D-Onshore seismics

A GEOFONCSOPORTOK HATÉKONYSÁGA HÁROMDIMENZIÓS SZEIZMIKUS MÉRÉSEKNÉL

Bernd THOMAS és Rolf PILLING

A háromdimenziós reflexiós mérések egyre szélesebb körben történő alkalmazása miatt újra tanulmányozni kell a geofoncsoportok irányfüggő tulajdonságait. A kétdimenziós szelvényezéssel ellentétben szükség van az azimutfüggő irányfüggőségi elemzésre. A szerzők bemutatnak három különböző geofoncsoportot és megvizsgálják az irányítottság, valamint a gyakorlati kivitelezés szempontjából.

ЭФФЕКТИВНОСТЬ ГРУППИРОВАНИЯ СЕЙСМОПРИЕМНИКОВ В ОБЪЕМНОЙ СЕЙСМОРАЗВЕДКЕ

Бернд ТОМАС и Рольф ПИЛЛИНГ

В связи с расширением области применения объемной сейсморазведки МОВ возникает необходимость в изучении зависимости параметров группирования сейсмоприемников от направления в пространстве. В отличие от обычного профилирования становится необходимым анализ зависимости параметров от азимутов. Авторами демонстрируются три различных типа группирования сейсмоприемников и исследуются их параметры с точки зрения ориентированности и практической осуществляемости.